

Air Force Institute of Technology

AFIT Scholar

Theses and Dissertations

Student Graduate Works

3-9-2005

Manufacture and Testing of an Activation Foil Package for Use in AFIDS

Warren E. Kimmel

Follow this and additional works at: <https://scholar.afit.edu/etd>



Part of the [Nuclear Engineering Commons](#)

Recommended Citation

Kimmel, Warren E., "Manufacture and Testing of an Activation Foil Package for Use in AFIDS" (2005). *Theses and Dissertations*. 3738.
<https://scholar.afit.edu/etd/3738>

This Thesis is brought to you for free and open access by the Student Graduate Works at AFIT Scholar. It has been accepted for inclusion in Theses and Dissertations by an authorized administrator of AFIT Scholar. For more information, please contact richard.mansfield@afit.edu.



**MANUFACTURE AND TESTING OF AN ACTIVATION FOIL PACKAGE FOR
USE IN AFIDS**

THESIS

Warren E. Kimmel
Captain, USA

AFIT/GNE/ENP/05-06

**DEPARTMENT OF THE AIR FORCE
AIR UNIVERSITY**

AIR FORCE INSTITUTE OF TECHNOLOGY

Wright-Patterson Air Force Base, Ohio

APPROVED FOR PUBLIC RELEASE; DISTRIBUTION UNLIMITED

The views expressed in this thesis are those of the author and do not reflect the official policy or position of the United States Air Force, Department of Defense, or the United States Government.

AFIT/GNE/ENP/05-06

**MANUFACTURE AND TESTING OF AN ACTIVATION FOIL PACKAGE FOR
USE IN AFIDS**

THESIS

Presented to the Faculty

Department of Engineering Physics

Graduate School of Engineering and Management

Air Force Institute of Technology

Air University

Air Education and Training Command

In Partial Fulfillment of the Requirements for the
Degree of Master of Science in Nuclear Engineering

Warren E. Kimmel, BS

Captain, USA

March 2005


APPROVED FOR PUBLIC RELEASE; DISTRIBUTION UNLIMITED

AFIT/GNE/ENP/05-06

**MANUFACTURE AND TESTING OF AN ACTIVATION FOIL PACKAGE FOR
USE IN AFIDS**

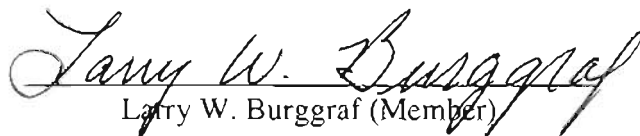
Warren E. Kimmel, BS
Captain, USA

Approved:



James C. Petrosky (Chairman)

09 MAR 05
date



Larry W. Burggraf (Member)

09 MAR 05
date



Richard A. Lillie (Member)

09 MAR 05
date

Abstract

This study used simulation and experiment to design and test foil packets for use in the Activation Foil Integrated Detection System (AFIDS). The initial plan to activate foil packets outside with the pulse reactor at White Sands Missile Range (WSMR) was not possible due to WSMR not having safety approval to take the reactor outside. As an alternative, the concept of using liquid nitrous oxide inside a reactor to simulate large volumes of air was investigated.

Simulation using the Standardized Computer Analyses for Licensing Evaluation (SCALE) program was used to select ten foils to be included in the foil packet. The size was selected with a target activity of 25 Bq for each foil four days after the activation when located 500 meters from a five kiloton equivalent nuclear weapon.

We analyzed whether N₂O could replicate large volumes of air in neutron transport experiments since one cubic centimeter of liquid N₂O contains as many molecules as 1371 cubic centimeters of air. A neutron propagating through the liquid N₂O should react like a neutron propagating through 1371 times as much air. Actual testing could not be completed at the Ohio State University Research Reactor due to hazardous levels of radiation in the facility during testing. The results of the simulation showed that pragmatic experimental factors inhibit use of the reactor in this way and an outside test is still required to provide the information Oak Ridge National Laboratory (ORNL) needs to validate the methodology used in Domestic Nuclear Event Attribution (DNEA).

Acknowledgments

I would like to express my sincere appreciation to my faculty advisor, Dr. James C. Petrosky, for his guidance and support throughout the course of this thesis effort. The patience, expertise and experience were certainly appreciated. I would also like to thank the other distinguished members of my committee, Dr. Larry W. Burggraf and Dr. Dick Lillie, their interest was appreciated and their expertise was invaluable.

I would like to thank laboratory technician, Mr. Eric Taylor, whose assistance, resourcefulness and knowledge were imperative to this project. I would also like to thank the staff of the Ohio State University research reactor for accommodating this research and providing valuable expertise and experience.

Most importantly, I thank my wife for keeping me focused and supporting my studies. Her sacrifices cannot be repaid but were certainly instrumental in any success I have enjoyed.

Warren E. Kimmel

Table of Contents

	Page
Abstract.....	iv
Acknowledgments.....	v
List of Figures.....	viii
List of Tables.....	x
I. Introduction.....	1
Background.....	1
Problem Statement.....	2
Scope.....	3
Assumptions/Limitations.....	3
Organization.....	5
II. Theory.....	6
Definitions.....	6
Effects of Nuclear Weapons.....	7
Activation.....	8
Neutron Detection.....	11
Gamma Detection.....	12
Gamma Spectroscopy.....	13
Neutron Sources.....	16
Liquid/Air Concept.....	16
ORNL Methodology.....	18
III. Foil Package Design.....	19
Foil Materials.....	19
Simulation of the Effect of Wire Shape on Neutron Activation.....	20
Foil Size.....	22
Foil Packaging.....	25
IV. Foil Package Activation and Spectroscopy.....	26
Gamma Spectroscopy.....	26
Low Level Activation Measurements.....	29

High Level Activation Measurements.....	31
V. Liquid Air Experiments	33
Liquid/Air Concept Simulation.....	33
Liquid/Air Experiment Design.....	34
Liquid/Air Experiment Simulation.....	37
Experiment	40
VI. Conclusions and Recommendations	46
Conclusions	46
Recommendations	48
Appendix A. Pu-Be Source.....	51
Appendix B. Gammas from Common Neutron Reactions	55
Appendix C. Point-to-Wire Solid Angle Comparison	64
Appendix D. Wire Activation Simulation Results.....	70
Appendix E. Calculation of N ₂ O Steel Cylinder Activation.....	72
Bibliography	79
Vita	82

List of Figures

Figure	Page
1. Activity of an activation foil where t_0 is the time of the foil's removal from the neutron flux.	10
2. Solid angle geometry for a point source.	15
3. Solid angle geometry for a circular disk.	15
4. Foil activation simulation geometry.	21
5. Detectors within the wire.	21
6. Foil package.	25
7. Activating foils with the Pu-Be source.	26
8. GENIE 2000 output showing the calibration equation fit from the multinuclide source.	28
9. Differential flux in OSU rabbit tube.	31
10. Nitrous oxide simulation.	33
11. Comparison of SCALE simulations for N ₂ O, air and liquid air.	34
12. Collimated OSU source experiment.	36
13. Collimating the OSU reactor to appear as a point source.	36
14. OSU reactor beam port simulation geometry.	37
15. OSU beam port characterization with poly plug and N ₂ O.	39
16. Characterization foils at end of beam port.	42
17. Neutron energy spectrum at end of OSU collimated beam port.	42
18. Shielding on end of OSU beam port.	44
19. N ₂ O in place at end of OSU beam port.	45

20. N ₂ O and air “equivalency”	48
21. 80 g Pu-Be source neutron energy spectrum.	54
22. Solid angle for a point source.	64
23. Point source solid angle vs. distance based on Knoll.	65
24. Solid angle geometry for a circular disk.	65
25. Approximation of solid angle for disk geometry based on Knoll.....	66
26. Approximation of disk solid angle vs. distance based on Knoll.....	67
27. Approximation of solid angle for disk geometry based on Ruby.	67
28. Approximation of disk solid angle vs. distance based on Ruby.	68
29. Geometry of cylinder at OSU beam port.	73
30. Using like triangles to solve projected height.....	73
31. Estimated area of activation.	74

List of Tables

Table	Page
1. Possible candidate materials for the AFIDS foil package.	19
2. Partial SCALE output of 1mm Al wire at 500 meters.	22
3. Determining foil size from projected activity.	23
4. Foils selected for experiment.	24
5. Multinuclide source for calibration.	27
6. Pu-Be activation results.	30
7. Rabbit tube activation results.	32
8. 4130 steel composition.	40
9. SAND-II input calculations.	41
10. M-1170 Pu-Be source calculator.	53
11. Common gammas from selected foils.	56
12. Point vs. disk solid angle comparison.	69
13. Calculations to determine wire size.	70
14. MCNP calculations to verify SCALE at 500 meters.	71

MANUFACTURE AND TESTING OF AN ACTIVATION FOIL PACKAGE FOR USE IN AFIDS

I. Introduction

Both parties in the 2004 Presidential Campaign Debates indicated that the most dangerous threat to the United States was a domestic nuclear event. Although no one likes to dwell on this scenario, we must be prepared to deal with one. Information about the device involved has not only political implications but is important in relief operations and public safety.

Background

A nuclear event requires analysis to determine weapon type and characteristics for use in Domestic Nuclear Event Attribution (DNEA). Much of this information can be gained from the prompt neutron spectrum of the weapon. Materials near the detonation will be activated by the prompt neutrons and information about the spectrum can be gained from the analysis of these activated materials.

One difficulty with using activated materials from near the detonation site is that the exact composition of the materials is unknown. The proposed Activation Foil Integrated Detection System (AFIDS) is a passive radiation detection system consisting of foil packages containing foils of known composition. The foils, located near the detonation, become activated by prompt neutrons from the nuclear detonation. Since the foils would be chosen to activate with neutrons at certain energy thresholds and the

reaction cross-sections are well known, the activity of the foils collected after a nuclear detonation would provide fluence and energy information about the neutron spectrum.

The neutron flux at a certain point can be calculated by computer adjoint calculations using a known neutron flux from a known source. In the case of an unknown source, if enough information is available from threshold activation measurements, it should be possible to unfold the neutron source spectrum using adjoint calculations. This method has been proven in and out of the laboratory in limited cases. Oak Ridge National Laboratory (ORNL) has developed a means for comparing an unknown spectrum to known spectra by comparing calculated activities from the known spectra using adjoint fluxes to measured activities of strategically placed foil packages. After a nuclear event, the activated foil packages would be collected, the neutron induced activity measured, and the results sent to ORNL. ORNL would then compare the measured activity to activity adjointly calculated from the known weapon spectra. The comparison would rank-order the closest matches to known spectra and eliminate weapons and types that do not match. The features of the most closely matched spectra would indicate types (e.g. uranium vice plutonium) and help to validate results from other methods such as fractionation analysis [22].

Problem Statement

The purpose of this thesis is to design, manufacture and test activation foil packages by simulation and testing in order to facilitate further research that provides several measured activities for ORNL to complete proof-of-principle verification for the methodology to be used in DNEA.

Scope

The original scope of this thesis was to design and build foil packages, irradiate them using the pulse reactor at White Sands Missile Range (WSMR), and compare the known spectrum found by adjoint calculations at ORNL. The WSMR pulse reactor does not have the safety approval for outside testing so the scope was modified to investigate the concept of using liquid nitrous oxide (N_2O) to replicate large volumes of air in lieu of outside testing at WSMR. Foil packages were designed, built and activated and neutron transport through N_2O was compared to neutron transport through air by simulation and experimentation at the Ohio State University (OSU) research reactor.

Assumptions/Limitations

The foils used are subject to physical and practical constraints. The atomic content of the foils has to be known so ORNL can do pre-calculations and time is not spent after retrieval determining the composition of the foils. The reactions of interest have to cover all parts of the neutron spectrum to include thermal, epithermal and fast neutrons. The cross-section of the reaction of interest has to be well documented to allow ORNL to perform calculations. To prevent self-absorption, the mean free path of the resulting gamma must be greater than the material thickness through which the gammas will be measured. For the purposes of packaging, the choice of foils was restricted to ones that are available in wire form.

Reactions of interest from neutron activation were limited to ones that produce gamma rays during decay to facilitate counting. Detectors used to measure the gamma activity of the foils should have resolution better than 10% full width at half maximum

(FWHM) and 1% absolute efficiency at 1 MeV. For design purposes, 1% absolute efficiency was assumed and 0.1 counts per second as the lower limit of counting based on counting with a High Purity Germanium (HPGe) detector for two hours. Foils were assumed located 500 meters from a five-kiloton nuclear weapon detonation and the activity measured four days after the nuclear event for design purposes. Since the lower limit of counting is 0.1 counts per second and assuming 100% decay percentage, 100% branching ratio, and 1% absolute efficiency, the minimum activity of the foil four days after activation must be at least 10 counts per second. The maximum activity of the foil four days after activation was limited to 1000 counts per second to minimize pile-up and dead time and to allow the same geometry for all foil counting. Higher activities can be counted by placing the foil farther from the detector but the system must then be recalibrated.

To locate a peak in gamma spectroscopy, the software used in this thesis uses the second differential to locate a peak, fits a gaussian to the peak, and provides the difference between data and background counts in standard deviations [6]. A standard deviation of three was assumed as the minimum detectable peak.

The foil packages are also subject to physical and practical constraints. They were designed to survive a five-kiloton nuclear detonation at 500 meters. This requires surviving 8 psi overpressure, 925°C, shock and blast. Since the exact location of the blast is unknown, the foil packages cannot be oriented towards the blast and must be designed to capture fast and epithermal neutrons from any direction. Direction is not as important for thermal neutrons because thermal neutrons reach equilibrium in velocity

and will backscatter into the foils. The foil packages should not present a hazard to the general population or the environment. Self-shielding within the packaging of the foils needs to be accounted for and minimized so each foil gets maximum exposure to the prompt neutrons. The cost per foil package needs to be low since a significant number of foil packages are needed to cover potential targets and low cost reduces pilfering. A limit of five dollars was assumed.

For the purposes of design, the simulated point source was monoenergetic at 14 MeV (upper energy limit of bomb neutrons) and yielded 10^{24} neutrons, approximately the equivalent of a five-kiloton weapon [14]. The duration of neutron production from a nuclear device is on the order of microseconds while the half-lives of the decay elements are on the order of hours or longer. Thus, the decay of the radionuclides during activation was assumed negligible and ignored when calculating activation.

Organization

A more in-depth analysis of the problem, design, simulation and testing procedures is discussed in the following chapters. Chapter II describes the theory behind nuclear weapon neutron output, foil activation and the methodology used by ORNL to compare neutron spectra. Chapter III provides the foil package design procedures and results while Chapter IV contains the testing procedures and results. Chapter V investigates the concept of using N_2O to replicate large volumes of air. Chapter VI contains conclusions and recommendations for future study. The appendices provide supporting calculations, tabulated data, and references used throughout the thesis.

II. Theory

Definitions

The following definitions are presented in the context that they are used in this thesis.

Foils.

Foils are the individual wires in the foil packet. They are chosen because of their ability to capture the neutrons in the energy range of interest.

Foil Packet.

Foil packets, or foil packages, are sets of foils packaged together. Foil packets are the physical entity deployed in the field.

Detectors.

For the purposes of this thesis, detectors refer to the devices used to measure the gamma rays being emitted from the activated foils. Detectors used in this thesis must have a minimum absolute efficiency of 1% and minimum resolution of 10% full width at half maximum. Detectors are not to be confused with foil packets.

SCALE.

Standardized Computer Analyses for Licensing Evaluation (SCALE) software is developed and maintained by ORNL under contract with the U.S. Nuclear Regulatory Commission and Department of Energy to perform criticality safety, radiation shielding, spent fuel characterization, and heat transfer analyses of nuclear fuel facilities and transport/storage package designs [23]. For the simulations in this thesis, the Shielding Analysis Sequence No. 4 (SAS4) was implemented. SAS4 is a control module that

allows calculation of radiation doses exterior to a transport/storage cask via a three-dimensional Monte Carlo analysis [27]. The output of SCALE is the product of neutron flux and a response function. Normally the response function is the factor to convert neutron flux to radiation dose. In this thesis, the response function was set to one when the required output was the neutron flux and set to the cross-section of the reaction of interest when the output was used for calculating activation. The fractional standard deviations in the output of SCALE are good indicators of whether the simulation is good or not. The goal is to get under 10% fractional standard deviation [4]. This can usually be achieved by adjusting the number of particles in the batches or the number of batches used in the Monte Carlo analysis.

Effects of Nuclear Weapons

A nuclear detonation is similar to a conventional explosion in that a large amount of energy is released within a limited space and time. This energy release drives the temperature and pressure up converting all materials present to hot, pressurized gasses. These gasses expand quickly and produce a shock or blast wave. A nuclear detonation differs from a conventional explosion in that much more energy is released in a shorter time with less mass. Much higher temperatures are achieved and more energy is emitted as heat and light (thermal radiation). For example, a foil package 500 meters from a ground burst of a 5 kT device will experience an overpressure of 8 psi and 50 cal/cm² of thermal radiation [8]. The 50 cal/cm² of thermal radiation translates to an increase of 900°C in silicon carbide assuming the radiation is absorbed in the first millimeter of material. A nuclear detonation also emits radiation called initial nuclear radiation or

prompt radiation. The radioactive substances left after the nuclear detonation continue to emit radiation that is known as residual radiation [8].

Nuclear fission (breaking apart of atoms) and fusion (combining of atoms) both release high-energy neutrons. A pulse of neutrons with energies of approximately 14 MeV and lower is emitted from the detonation and is called the prompt spectrum. These neutrons activate the foil packages based upon their energy.

Radiation diffuses as it propagates outward from a point source. The direct (unscattered) fluence is given by

$$\Phi = \frac{N}{4\pi d^2}, \quad (1)$$

where N is the number of neutrons and d is the distance from the source [12]. Thus, a point source of 10^{24} neutrons (e.g. a 5 kT device) would have an unscattered fluence of approximately 8×10^{14} n cm⁻² at 100 meters, 3×10^{13} n cm⁻² at 500 meters and 1.3×10^{12} n cm⁻² at 2500 meters.

Activation

Activation foils work using the physics of neutron absorption in isotopes to produce radionuclides. These daughter radionuclides then decay by emitting alpha or beta particles, or gamma rays. The emitted particles or rays can then be detected and the activity of the foil can be determined. The activity can be calculated from

$$A = \lambda N_0, \quad (2)$$

where λ is the decay constant and N_0 is the number of activated atoms.

The change in the number of activated nuclei is the rate of production minus the rate of decay. Mathematically this is

$$\frac{dN}{dt} = \phi\sigma N_T - \lambda N, \quad (3)$$

where $\phi\sigma N_T$ is the rate of production and λN is the rate of decay or activity. The number of radioactive nuclei is represented by N , ϕ is the flux of neutrons, σ is the absorption cross-section, N_T is the number of target nuclei and λ is the decay constant [28]. The absorption cross-section is material and energy dependent. A thermal material has a large absorption cross-section in the thermal region and a threshold material has a large cross-section or resonance at specific energies above the thermal region (0.5 eV). Therefore, a thermal reaction of interest would be initiated by thermal neutrons and a threshold reaction of interest would require a neutron with an energy corresponding to its threshold to initiate the reaction.

The pulse length of neutrons from a bomb is much less than a second and the half-lives of the radionuclides of interest are in the range of hours to years so the decay during activation is negligible and can be ignored. Thus, the number of radionuclides produced from the pulse can be calculated by

$$N_0 = n\sigma N_T, \quad (4)$$

where N_0 is the number of radionuclides produced and n is the number of neutrons incident on the target. Because no activation occurs during decay, the decay can be accounted for by

$$N(t) = N_0 e^{-\lambda t}, \quad (5)$$

where t is the time after activation [13].

When a material with an absorption cross-section is exposed to a constant neutron flux, the induced activity builds with time and approaches a saturation activity A_{inf} as shown in Figure 1. In this example, neutron irradiation has proceeded for a time t_0 when the foil is removed from the neutron flux with an activity A_0 . This leads to a saturation activity given by

$$A_{\text{inf}} = \frac{A_0}{(1 - e^{-\lambda t_0})}. \quad (6)$$

Once removed from the neutron flux the radioactivity will decay by Equation 5.

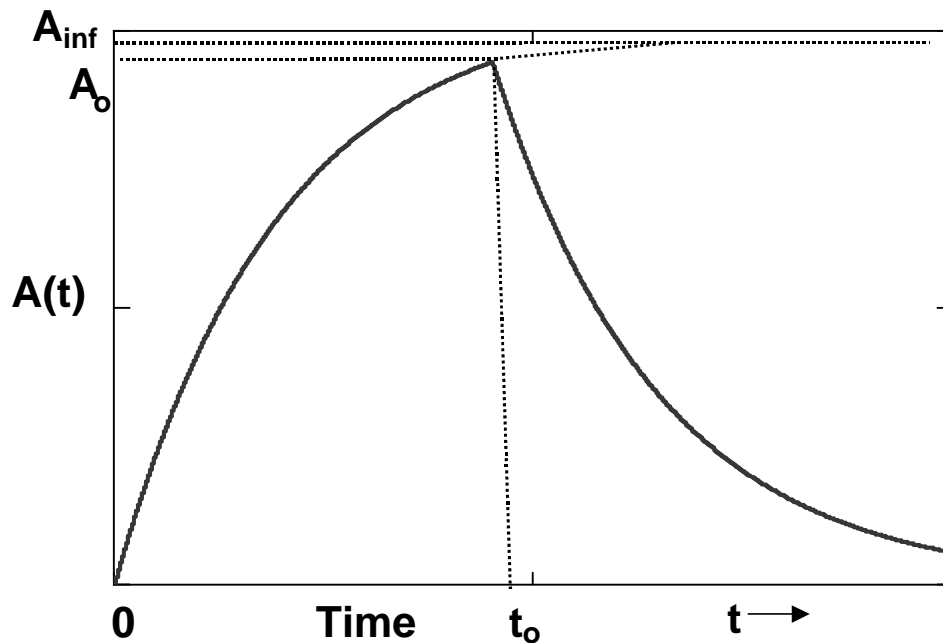


Figure 1. Activity of an activation foil where t_0 is the time of the foil's removal from the neutron flux [12].

In the case of a nuclear detonation, a variety of materials with absorption cross-sections will activate with exposure to the neutron flux. The composition of these

materials is unknown so the starting point for activation is unknown. The elements used in the AFIDS foils may be common in many materials but might not be present in combinations or concentrations, may be shielded so as to mask parts of the spectrum, or would require separation techniques which reduce or eliminate the accuracy of the measurements.

Neutron Detection

Radiation detection typically requires conversion of radiation energy into electrical energy. However, neutron detection differs from other detection methods because the neutrons have no charge. Therefore thermal neutron detectors rely upon neutron induced nuclear reactions to produce a secondary charged particle that can then be counted by charged particle detectors [30]. Although these detectors can detect neutrons by producing a prompt output pulse, they are not practical for AFIDS as the cost of the detector alone prohibits mass fielding. They are also manpower intensive so even if the detector survived the effects of a nuclear detonation, the operator might not.

Neutron measurements can also take advantage of the radioactivity induced in some materials by neutron interactions. Foils made of materials selected for their ability to activate with neutrons can be exposed to a flux of neutrons, collected later, and then the induced radioactivity can be counted using conventional means such as gamma spectroscopy. This passive method meets AFIDS' needs of low cost, low maintenance, nuclear event survivable, and delayed counting.

Gamma Detection

Two common types of detectors found in the lab for measuring gamma rays are inorganic scintillators (e.g. NaI(Tl)) and semiconductor detectors (e.g. HPGe). The two main factors in choosing between them are energy resolution and counting efficiency. Energy resolution is a measure of the ability to discern fine detail in the incident energy of the radiation. Absolute counting efficiency is the ratio of gamma rays detected to the total gamma rays emitted by the source. It is dependent on the geometry of the setup and the energy of the gamma rays as well as the detector. In comparing the two detectors, NaI(Tl) detectors tend to have better counting efficiency while HPGe detectors have better resolution [12]. Normal absolute efficiencies for HPGe detectors of 800 keV gamma rays are around one percent [7, 19]. Absolute efficiencies of NaI(Tl) detectors are typically about an order of magnitude better [12]. Typical resolution of an HPGe detector is 1.95 keV FWHM at 1.33 MeV and the normal resolution of an NaI(Tl) detector is about an order of magnitude worse. Better efficiency gives more counts while the better resolution may let multiple foils be counted simultaneously. Either type of detector should work to measure AFIDS foil packages and should be available throughout the country at colleges and universities if provision and planning are made for their calibration and use.

The detector used in this research was a Canberra Model GC10021. The Canberra Model GC10021 HPGe detector is a p-type, closed-end, coaxial detector that detects gamma activity from low activity foils. The crystal has dimensions of 83 millimeters diameter and 84.5 millimeters length. The detector was configured so that

the front crystal face was located 5 millimeters from the detection window [30]. The detector collects electrical charges created at either boundary of the semiconductor material, and the spectroscopy system records these pulses and differentiates between energies. The detector was located in a model 747 Canberra Lead Shield. The shield blocks high background gamma radiation by using a four-inch thick lead wall and a 1.0-millimeter tin and 1.6-millimeters copper graded liner. The tin and copper liner prevents interference by lead x-rays [5].

The detector used at the OSU research reactor was also an HPGe. The volume of the crystal is approximately 60 cubic centimeters [26].

Gamma Spectroscopy

Energy and efficiency calibration of the detector to a known source is essential for accurate measurements. Once calibrated, an unknown source can be measured with a high degree of accuracy provided the factors that can impact the count are accounted for.

Absolute efficiency is the ratio of the number of gamma rays counted to the number of gamma rays emitted by the source. It is represented by

$$\frac{N_C}{N_E} = f_\gamma f_w f_g f_{bs} \epsilon_{\text{int}} , \quad (7)$$

where N_C is the number of gamma rays counted, N_E is the number of gamma rays emitted by the source, f_γ is the self-absorption correction factor, f_w is the detector window correction factor, f_g is the geometry correction factor, f_{bs} is the back scatter correction factor and ϵ_{int} is the intrinsic efficiency of the detector itself.

Self-absorption is the absorption of gamma rays by the source itself. The mean free path of a gamma in a material is the average distance it travels before interacting. Self-absorption can be a problem if the mean free path of the gamma is smaller than the thickness of the foil. The mean free path is calculated by

$$\lambda = \frac{1}{\frac{\mu}{\rho} * \rho} , \quad (8)$$

where λ is the mean free path, μ is the macroscopic cross-section and ρ is the density [28]. Self-absorption is usually accounted for by empirical formulas based on experimental results. Equation 9 is an example of an empirical gamma self-absorption correction factor for gold where t is in mils [25].

$$f_{\gamma} = 1.0 + \frac{t}{239.5} \quad (9)$$

The detector window correction factor, f_w , corrects for the number of gamma rays absorbed or scattered by the detector window. This factor is normally very close to unity for a thin window and the detector efficiency typically includes this correction factor.

Backscattering of gamma rays from surrounding materials can increase the count rate. This factor (f_{bs}) is also normally very close to unity.

The counter geometry correction factor, f_g , corrects for the fraction of the radiation that is not subtended by the detector and is defined as

$$f_g = \frac{\Omega}{4\pi} , \quad (10)$$

where Ω is the solid angle that is subtended by the detector. For a point source located along the axis of a right circular cylindrical detector, Figure 2, the solid angle (in steradians) is given by

$$\Omega = 2\pi\left(1 - \frac{d}{\sqrt{d^2 + a^2}}\right), \quad (11)$$

where d is the source-detector distance and a is the detector radius.

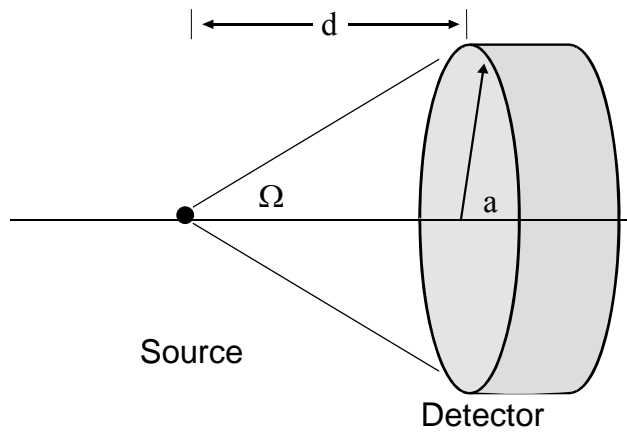


Figure 2. Solid angle geometry for a point source.

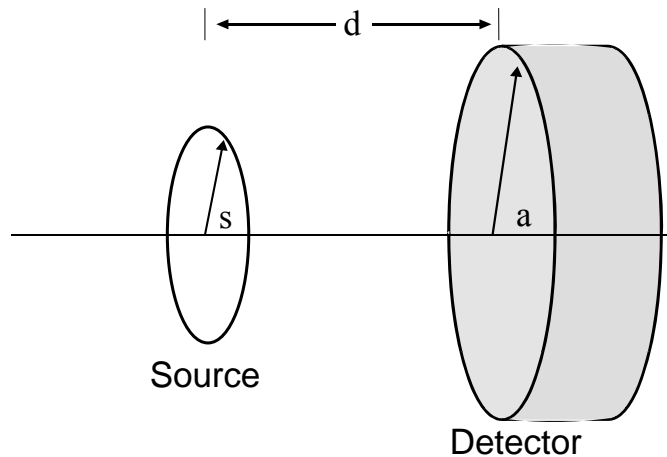


Figure 3. Solid angle geometry for a circular disk.

A circular disk source as shown in Figure 3 has a more complex solution to the solid angle. Using s as the radius of the source, it has been shown that

$$\Omega = \frac{2\pi a}{s} \int_0^{\infty} \frac{e^{-dk} J_1(sk) J_1(ak)}{k} dk, \quad (12)$$

where the $J_1(x)$ are Bessel functions of x [12].

Neutron Sources

Since actual nuclear bomb testing is unrealistic, alternate neutron sources must be considered. A good source for replicating a neutron bomb should yield as many fast neutrons as possible and be capable of operating in a controlled outdoor setting, which would be ideal to represent the air-over-ground transport with the associated ground and sky shine.

Two sources were used in this thesis. A 300 μCi plutonium-beryllium (Pu-Be) source was used for low level neutron irradiation and the 500 kW Ohio State University research reactor was used for higher level neutron irradiation. Further information on the Pu-Be source used and the calculated activity is contained in Appendix A.

The OSU research reactor is an open pool type light water reactor. The fuel is aluminum clad U_3Si_2 enriched to 19.5% ^{235}U with a ^{235}U loading of approximately 3.9 kg. The pool holds approximately 5700 gallons of water and is the primary coolant with a secondary cooling loop containing ethylene glycol and water. The integral neutron flux near the core has been measured to be $2 \times 10^{12} \text{ n cm}^{-2} \text{ s}^{-1}$ at full power [26].

Liquid/Air Concept

In the case where a source cannot be taken outside, the distance and scattering mechanisms must be simulated or engineered. This could be accomplished by placing a depth of liquid between the source and the foil packets. The theory behind this is that the

liquid is much denser than air so with the correct geometry the number of molecules encountered by the neutrons passing through the liquid would be equivalent to the number of molecules encountered by the neutrons passing through air for a much greater distance. For example, the density of dry air is approximately 0.0011 g cm^{-3} . The density of liquid air is approximately 0.89 g cm^{-3} . The ratio of the density of liquid air to the density of dry air yields a factor of 809. Thus, 1 centimeter of liquid air should appear as 8.09 meters of dry air to a neutron. Another method is to use the number of atoms in a cm^3 . This can be calculated by

$$N = \frac{\rho N_A V}{AW} (\%), \quad (13)$$

where ρ is the density, N_A is Avogadro's constant, V is volume, AW is the atomic weight and (%) is the percentage of occurrence in the molecule. Using Equation 13, liquid N_2O has 6.3×10^{22} atoms and air, modeled as 78% nitrogen and 22% oxygen with a density of 1.1 mg/cm^3 , has 4.6×10^{19} atoms per cm^3 . This gives a ratio of 1371 or 1 cm of liquid N_2O should appear as 13.71 meters of air. Simulation with SCALE indicated that neither method is correct as they do not take into account the true path of a neutron moving through a substance.

Sky shine, the scattering of neutrons from the air above, should still be appropriately replicated in liquid air, provided the height of the liquid air is sufficient to reflect all neutrons before they escape from the container. Other liquids closely resembling air theoretically could be used but scattering will differ depending upon the atomic concentrations (e.g. heavier atoms scatter differently than lighter atoms). Using liquid to replicate air in depth also has the added advantage of having more neutrons

available at the experiment if the same source is used. The flux from an isotropic source decreases by the square of the distance away from the source. Using a volume of liquid to replicate a volume of air removes the distance-squared factor because of the smaller distance traveled by the neutron. Thus, a much higher flux can be attained while still accounting for scattering through a large distance of air. To apply the distance-squared factor to a flux measured at a detector near the source, multiply by

$$\frac{d_1^2}{d_2^2}, \quad (14)$$

where d_1 is the distance from the source to the near detector and d_2 is the distance from the source to the point desired.

ORNL Methodology

ORNL has developed a computer code to compare an unknown neutron spectrum to a database of known neutron weapon spectra and rank-order the best fit. Prior to any detonation, air-over-ground adjoint radiation transport calculations are performed for each type of known foil and the results stored. After a detonation, as many foils as possible are recovered and then measured to determine saturation activity. Once the detonation location is known, the calculated saturated activity for each foil is obtained by folding all the known weapon leakage spectra with the pre-calculated adjoint fluences at the detonation location. The calculated and measured activities can now be compared and the most probable weapon spectra determined by least squares fitting [22].

III. Foil Package Design

This chapter presents the design of the foil packages starting with the selection of the foil materials to be considered. Simulations using SCALE were used to check the effect of wire geometry on activation and to determine the size of the foils. The chapter concludes with the packaging of the selected foils.

Foil Materials

The foils considered for use in the foil packages are listed in Table 1. It is based on simulations at ORNL and includes reactions of interest that give as complete coverage of the neutron spectrum as is possible [22].

Table 1. Possible candidate materials for the AFIDS foil package [3, 15, 18, 28].

Reaction	Half-Life	γ energy [keV]	Threshold [MeV]	Wire Form	γ mean free path [cm]
$^{27}\text{Al}(n,\alpha)^{24}\text{Na}$	14.95 h	<u>1369</u> , 2754	6.5	Y	7.0
$^{197}\text{Au}(n,2n)^{196}\text{Au}$	6.18 d	356, <u>333</u> , 426	8.06	Y	0.16
$^{59}\text{Co}(n,\gamma)^{60}\text{Co}$	5.271 y	1333, <u>1173</u>	thermal	Y	2.0
$^{133}\text{Cs}(n,p)^{133}\text{Xe}$	5.243 d	<u>81</u>	3.0	N	0.14
$^{127}\text{I}(n,2n)^{126}\text{I}$	13.0 d	<u>389</u>	10.0	N	1.6
$^{115}\text{In}(n,n')^{115}\text{In}$	4.486 h	<u>497</u>	.369	Y	1.5
$^{139}\text{La}(n,\gamma)^{140}\text{La}$	1.678 d	1596, 487, 816, <u>329</u>	thermal	N	0.92
$^{55}\text{Mn}(n,2n)^{54}\text{Mn}$	312.1 d	<u>835</u>	10.4	Y	2.1
$^{181}\text{Ta}(n,\gamma)^{182}\text{Ta}$	114.43 d	<u>68</u> , 1121	thermal	Y	0.0052
$^{51}\text{V}(n,\alpha)^{48}\text{Sc}$	43.7 h	<u>984</u> , 1312, 1038	9.0	Y	2.8
$^{58}\text{Ni}(n,2n)^{57}\text{Ni}$	35.6 h	<u>1378</u>	12.4	Y	2.1
$^{58}\text{Ni}(n,p)^{58}\text{Co}$	70.88 d	<u>811</u>	2.09	Y	1.6
$^{56}\text{Fe}(n,p)^{56}\text{Mn}$	2.578 h	<u>847</u> , 1811, 2113	4.9	Y	1.9
$^{54}\text{Fe}(n,p)^{54}\text{Mn}$	312.1 d	<u>835</u>	thermal	Y	1.9
$^{63}\text{Cu}(n,\alpha)^{60}\text{Co}$	5.271 y	1333, <u>1173</u>	6.13	Y	3.5
$^{63}\text{Cu}(n,\gamma)^{64}\text{Cu}$	12.701 h	<u>1346</u>	thermal	Y	3.5

The mean free path in Table 1 is calculated using Equation 8 and the corresponding underlined gamma energy. Self-absorption was considered unacceptable if the gamma mean free path was shorter than the foil (wire) diameter. The mean free path of the 68 keV gamma from tantalum (branching ratio of 2.65) is too short but the 1.121 MeV gamma (branching ratio of 34.9) has a mean free path longer than 1 mm.

The physical characteristics of the foil are a significant consideration in the choice of foils. For example, cesium with a 3 MeV threshold reaction is not available as a wire and is pyrophoric. Additionally, cesium activates and becomes xenon, a noble gas that is difficult to contain. Iodine, lanthanum and manganese are also not available as wires but manganese is available as 80% manganese / 20% copper wire and lanthanum is available in a foil that can be sliced into wires. Iodine was not chosen for this design but could be pelletized and considered in future studies.

Simulation of the Effect of Wire Shape on Neutron Activation

The neutron flux is attenuated by atoms in the materials, resulting in non-uniform activation of the sample. For this reason, foils used for activation analysis are typically very thin wires or circular discs that are oriented toward the source so the flux penetrates through the material with little attenuation and the activation is relatively uniform. Using the point detectors available in SCALE within a wire allows comparison of the activation. A 1 mm thick aluminum wire 1 cm long was simulated 500 m from a 14 MeV point source as shown in Figure 4. Nine detectors were positioned within the cross-section of the wire as shown in Figure 5.

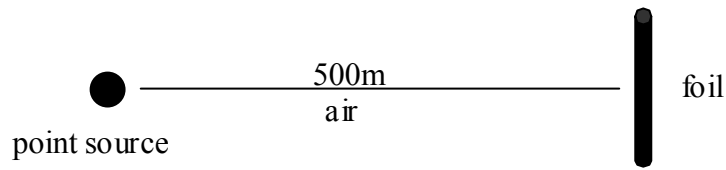


Figure 4. Foil activation simulation geometry.

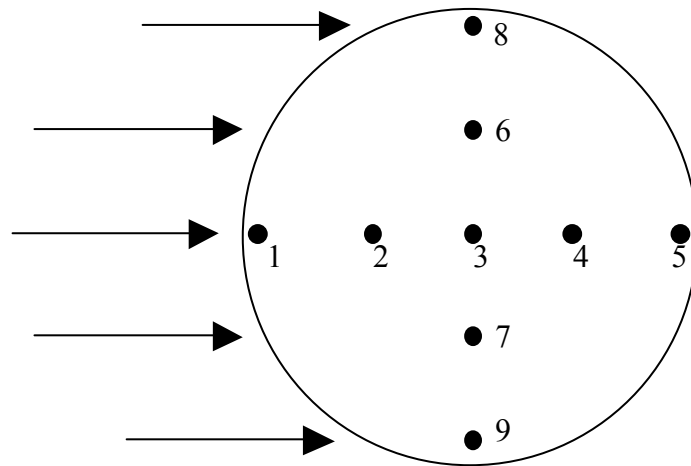


Figure 5. Detectors within the wire.

SCALE uses the Monte Carlo method for neutron transport and thus has statistical error. One hundred batches of 1000 particles were required to keep the statistical error below 10%. If the variation among the detectors is greater than the statistical error, the flux cannot be considered uniform. If the flux is uniform, one detector can be placed anywhere in the wire for future simulations.

The total response column in Table 2 represents the activation of the aluminum at the detector location as a result of the flux being multiplied by the cross-section of aluminum. The fractional standard deviations (fsd) are all within 4.5%. The difference between detector 7, the lowest, and detector 4, the highest, is just 1.7%, well within the fractional standard deviation. This allows one detector to be placed in the wire for future simulations.

Table 2. Partial SCALE output of 1mm Al wire at 500 meters.
responses(detector)

detector	uncoll response	fsd uncoll	total response	fsd total
1	9.6×10^{10}	1.8×10^{-3}	6.5×10^{11}	4.4×10^{-2}
2	9.2×10^{10}	1.9×10^{-3}	6.5×10^{11}	4.4×10^{-2}
3	9.3×10^{10}	2.0×10^{-3}	6.5×10^{11}	4.5×10^{-2}
4	9.8×10^{10}	1.8×10^{-3}	6.6×10^{11}	4.5×10^{-2}
5	9.4×10^{10}	1.8×10^{-3}	6.5×10^{11}	4.4×10^{-2}
6	9.3×10^{10}	2.0×10^{-3}	6.5×10^{11}	4.4×10^{-2}
7	9.3×10^{10}	2.0×10^{-3}	6.5×10^{11}	4.3×10^{-2}
8	9.3×10^{10}	2.0×10^{-3}	6.5×10^{11}	4.3×10^{-2}
9	9.3×10^{10}	2.0×10^{-3}	6.5×10^{11}	4.4×10^{-2}

Foil Size

Another limitation on the foils was that activity had to be measurable four days after activation. Simulations were used to determine the size of foil needed to obtain this. The simulations were run on each type of foil at 500 m from the source. Air was configured as 78% nitrogen and 22% oxygen with a density of 1.1 mg/cm^3 . The foils were right circular cylinders, 1 mm in diameter, 1 cm long and centered at the simulated distance standing upright as shown in Figure 4. A point source was simulated having 10^{24} neutrons and energy of 14 MeV.

The SCALE results were used to calculate the activity four days after the activation. The sizes of the wires were adjusted to attain an activity between the minimum for the particular wire and 1000 Bq. The complete spreadsheet is in Appendix D and the significant results are presented in Table 3.

Table 3. Determining foil size from projected activity.

	(σφ) SCALE [n/s]	radius [cm]	length [cm]	mass [mg]	Initial A [Bq]	T _{1/2} [days]	A at +4 days [Bq]	Min. A [Bq]
Al								
500 m	6.26 x 10 ⁻¹³	0.05	1.00	21.20	3815.97	0.62	44.56	10.0
330 m	3.24 x 10 ⁻¹²	0.05	0.05	1.00	932.27	0.62	10.89	10.0
700 m	2.07 x 10 ⁻¹³	0.05	1.00	21.20	1259.02	0.62	14.70	10.0
800 m	7.64 x 10 ⁻¹⁴	0.05	1.00	21.20	465.41	0.62	5.44	10.0
Au								
500 m	9.46 x 10 ⁻¹²	0.05	0.30	45.47	1707.56	6.18	1090.37	12.4
1100 m	1.85 x 10 ⁻¹³	0.05	0.30	45.47	33.33	6.18	21.28	12.4
1200 m	6.22 x 10 ⁻¹⁴	0.05	0.30	45.47	11.22	6.18	7.17	12.4
Co								
500 m	6.24 x 10 ⁻¹¹	0.05	1.00	69.90	185.90	1923.92	185.63	10.0
1100 m	3.80 x 10 ⁻¹²	0.05	1.00	69.90	11.33	1923.92	11.31	10.0
1200 m	8.38 x 10 ⁻¹³	0.05	1.00	69.90	2.50	1923.92	2.49	10.0
In								
100 m	1.22 x 10 ⁻⁹	0.05	1.00	57.41	1.58 x 10 ⁷	0.19	5.73	23.0
500 m	2.49 x 10 ⁻¹¹	0.05	1.00	57.41	3.22 x 10 ⁶	0.19	0.12	23.0
La								
500 m	1.15 x 10 ⁻¹¹	0.05	0.50	24.13	5747.28	1.68	1101.60	10.5
1600 m	2.72 x 10 ⁻¹³	0.05	0.50	24.13	136.26	1.68	26.12	10.5
1700 m	1.32 x 10 ⁻¹⁴	0.05	0.50	24.13	6.62	1.68	1.27	10.5
Mn 80%								
500 m	2.71 x 10 ⁻¹²	0.05	1.50	68.80	52.60	312.10	52.14	10.0
700 m	5.23 x 10 ⁻¹³	0.05	1.50	68.80	10.14	312.10	10.05	10.0
Ta								
500 m	3.83 x 10 ⁻¹⁰	0.02	0.50	9.44	844.82	114.43	824.60	28.7
1000 m	6.65 x 10 ⁻¹¹	0.02	0.50	9.44	146.42	114.43	142.91	28.7
1100 m	1.33 x 10 ⁻¹¹	0.02	0.50	9.44	29.33	114.43	28.63	28.7
V								
500 m	6.23 x 10 ⁻¹⁴	0.05	1.00	47.99	155.61	1.82	33.95	10.0
600 m	3.38 x 10 ⁻¹⁴	0.05	1.00	47.99	84.41	1.82	18.42	10.0
700 m	1.60 x 10 ⁻¹⁴	0.05	1.00	47.99	40.00	1.82	8.73	10.0
Ni cross-section for (n,p)								
500 m	3.67 x 10 ⁻¹²	0.05	1.00	69.92	298.12	70.88	286.68	10.1
1000 m	1.57 x 10 ⁻¹³	0.05	1.00	69.92	12.74	70.88	12.25	10.1
1100 m	9.82 x 10 ⁻¹⁴	0.05	1.00	69.92	7.97	70.88	7.67	10.1
Cu cross-section for (n,a)								
250 m	1.61 x 10 ⁻¹²	0.05	2.00	140.74	8.93	1923.92	8.92	10.0
500 m	1.51 x 10 ⁻¹³	0.05	2.00	140.74	0.84	1923.92	0.84	10.0

The wires chosen for further experimentation are listed in Table 4 along with their dimensions. Iron did not have enough activation with reasonable size to be measured

four days after an event so was not pursued as a foil in further experiments. The activity of indium was also below the minimum of 23 Bq due to the short half-life but could still be useful if collected early enough. Most of the wires were chosen with a length of 1 cm but gold was shortened to 3 mm to reduce its activation to near 1000 Bq, this also kept the cost down. The foil length was limited to 3 mm to keep it upright in the glass tubes used to package the foils. The length the manganese/copper wire was set at 1.5 cm to assist the activity of both. The tantalum wire was set to 0.5 cm to keep activity under 1000 Bq. Copper did not meet the minimum activation but two wires of 1 cm each were chosen as it is relatively inexpensive. Table 3 also contains the expected distance from the source the foil was expected to perform. For example, vanadium should perform as designed to between 600 and 700 meters as it activated to 18.42 Bq at 600 meters but only 8.73 Bq at 700 meters.

Table 4. Foils selected for experiment.

<u>Element</u>	<u>diameter</u> <u>[mm]</u>	<u>length each</u> <u>[cm]</u>
Al	1	1
Au	1	0.3
Co	1	1
In	1	1
La	1	0.5
Mn - Cu	1	1.5
Ta	0.38	0.5
V	1	1
Ni	1	1
Cu	1	2

A check on the simulation was done using MCNP to simulate a 1 mg Al wire at 500 meters. The MCNP results and corresponding calculations are in Appendix D. SCALE gave 1.4×10^7 atoms activated and MCNP yielded 1.7×10^7 . The results were

within 18%. This check was done to see if SCALE was being implemented properly and results were realistic before ordering the wires.

Foil Packaging

The geometry shown in Figure 6 meets the 360-degree coverage limitation while keeping the foils from shielding themselves or each other. Initial planning has the foil packages placed on high structures such as building tops and cell phone towers to maximize exposure.

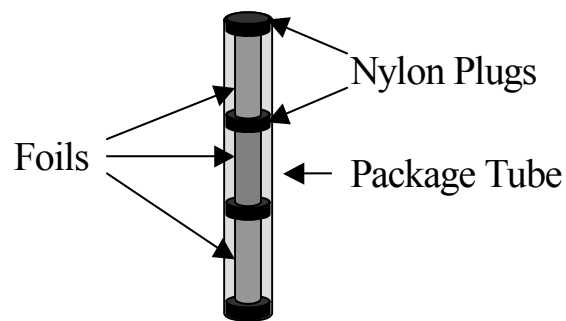


Figure 6. Foil package.

The packaging should also not shield the foils or it may change the spectrum for activation. Silicon carbide would make an ideal packaging material with a melting point of 1825°C, a modulus of rupture of 9500 psi, and a low absorption cross-section [24]. The glass tubes used in this thesis contained sodium that activated and were too fragile to survive in the field.

IV. Foil Package Activation and Spectroscopy

This chapter presents the results of foil package activation and spectroscopy measurements. The gamma spectroscopy systems used were calibrated against each other and the accuracy of measuring wires as point sources investigated. The foils were activated to a low level to check for complications in gamma spectroscopy and then the foil packages were activated to a higher level to test performance.

Gamma Spectroscopy

Foils had to be activated to perform gamma spectroscopy experiments. They were activated locally using a Pu-Be source. The Pu-Be source is contained in a barrel approximately 45 cm high and 36 cm in diameter. The barrel is filled with paraffin and has a hollow center core approximately 10 cm in diameter. The source is stored at the bottom of the hole, approximately 21.5 cm from the end of the barrel. Wires were activated with the Pu-Be source container lying on its side and the wires contained in foil packets located over the open end as shown in Figure 7. The neutron flux at the foil location was $1.9 \times 10^3 \text{ n cm}^{-2} \text{ s}^{-1}$ as calculated in Appendix A.

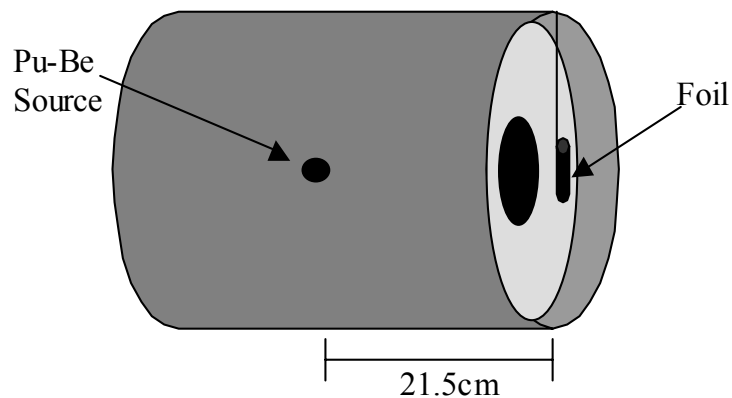


Figure 7. Activating foils with the Pu-Be source.

Spectroscopy System Calibration.

Accurate spectroscopy requires energy and efficiency calibration. If the calibration is done in the same geometry as the measuring and the sources are similar, no correction factors need to be applied. The HPGe detector system with the Genie 2000 software [6] was calibrated using a multi-nuclide source consisting of the isotopes in Table 5 with a reference date of 15 July 2004. The gamma spectrum was measured using the same geometry proposed for the wires (1 mm off the detector face), including background subtraction.

Table 5. Multinuclide source for calibration.

<u>Nuclide</u>	<u>Half Life (d)</u>	<u>Initial Activity (γ/s)</u>	<u>γ (keV)</u>
²⁴¹ Am	157742.1	387.9	60.0
¹⁰⁹ Cd	462.2	572.2	88.0
⁵⁷ Co	271.8	484.3	122.1
¹³⁹ Ce	137.6	580.3	165.9
²⁰³ Hg	46.6	1845	279.2
¹¹³ Sn	115.1	1797	391.7
⁸⁵ Sr	64.8	3431	514.0
¹³⁷ Cs	11012.1	2165	661.6
⁸⁸ Y	106.6	5151	898.0
⁶⁰ Co	1924.3	2989	1173.2
⁶⁰ Co	1924.3	2993	1332.5
⁸⁸ Y	106.6	5447	1836.0

A 1 cm Cu-Mn wire (1 mm diameter) was activated for 30 hours to compare AFIT's spectroscopy system with OSU's spectroscopy system. The wire was chosen for the large thermal cross-section of the ⁵⁵Mn(n, γ)⁵⁶Mn reaction and the 2.578 hour half life. This combination allowed the wire to be irradiated to saturation with the Pu-Be source locally and then transported to OSU for gamma spectroscopy with measurable activity. The OSU system had been calibrated with a 1 mm diameter, 1 cm long cobalt wire source

from the National Institute of Standards and Technology (NIST) [26]. The activity calculated by the OSU spectroscopy system for the Cu-Mn wire was 5.53 becquerel (Bq) \pm 15.95% at the time the wire was removed from the Pu-Be source. After another activation to saturation with the Pu-Be source, the wire was measured on the AFIT spectroscopy system. The activity of 4.775 ± 0.313 Bq was within the 15.95% error of the 5.53 Bq measured at OSU. The experiment was repeated using a gold wire resulting in activities of $4916 \text{ Bq} \pm 3.25\%$ at OSU and 5116 ± 143 Bq at AFIT. These results were also within the error limits. The efficiency calibration used is shown in Figure 8.

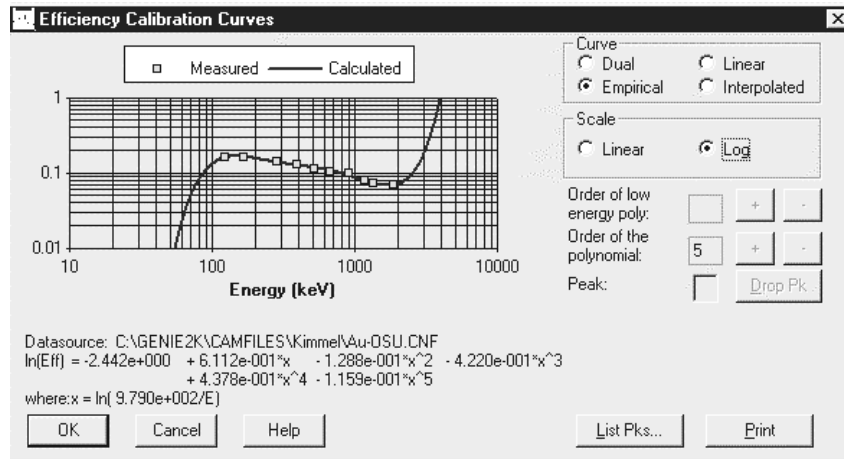


Figure 8. GENIE 2000 output showing the calibration equation fit from the multinuclide source.

Wire vs. Point.

A comparison of the solid angle using Equations 11 and 12 (Appendix C) indicated that a wire source could not be measured exactly as a point source. However, at 1 mm off the detector surface, the difference in solid angle between a point and a 1 cm wire is less than 0.1%. Since this amount of error is negligible when compared to the

normal statistical error of the spectroscopy system (greater than 1%), the wire could be calibrated and measured as though it were a point source.

To experimentally validate this conclusion, a 1 cm gold wire was activated by the Pu-Be source and measured. The activity was measured at $5.184 \times 10^{-4} \pm 1.84 \times 10^{-5} \mu\text{Ci}$. The wire was then rolled into a sphere approximately 2 mm in diameter to more closely resemble a point source and measured again. The result was an activity of $4.563 \times 10^{-4} \pm 1.58 \times 10^{-5} \mu\text{Ci}$. These results do not correspond within error bounds but when Equation 9 is applied to compensate for self-absorption in gold, the results become $5.321 \times 10^{-4} \pm 1.84 \times 10^{-5} \mu\text{Ci}$. These results correspond within the error and confirm that the difference between measuring a point source and a 1 cm wire source at the face of the detector is insignificant, backing up the solid angle comparison in Appendix C.

Low Level Activation Measurements

The foils were activated with a 15-hour irradiation by the Pu-Be source to check for gamma producing reactions that could interfere with the gamma spectroscopy of the reactions of interest. The foils received a neutron fluence on the order of $1 \times 10^8 \text{ n cm}^{-2}$ and only three reactions were detected in two hour counts as shown in Table 6. The indium reaction (54 minute half-life) and manganese reaction (2.5 hour half-life) would both decay prior to gamma spectroscopy on the reactions of interest. The gold reaction (2.7 day half-life) would still be present at foil recovery but the reaction of interest for gold (n,2n) has a half-life of 6.2 days so the longer the delay in counting, the easier it would be to detect the (n,2n) reaction over the (n, γ) reaction.

Table 6. Pu-Be activation results.

<u>Element</u>	<u>Primary Gammas Detected (keV)</u>	<u>Reaction</u>	<u>Activity (μCi)</u>
Ni	None		
La	None		
Cu	None		
V	None		
Ta	None		
Co	None		
In	417, 819, 1098, 1294, 2113	n, γ	6.67×10^{-5}
Al	None		
Au	411	n, γ	4.53×10^{-6}
Mn	846, 1810	n, γ	4.48×10^{-5}

The four most common neutron reactions, (n, γ), (n,2n), (n,p) and (n, α), were researched for each foil and the half-life, decay method and percentage, branching ratio and gamma energy for each were tabulated in Appendix B. The list was then sorted by gamma energy and possible spectroscopy conflicts could be isolated. The screening criterion was that any two gammas with peaks within 2 keV of each other would not be measured together since the resolution of an HPGe detector is ~ 2 keV FWHM at 1.3 MeV. Copper, cobalt and nickel have reactions that produce the same nuclide and tantalum and gold have reactions that produce several gammas that are within 2 keV of each other. Nine more combinations of materials had gammas within 2 keV but by grouping the wires into three groups for measuring, all but one combination can be avoided. The 136 keV gamma is common with nickel and gold. The nickel is a second-generation decay and gamma from the gold comes from a metastable state and has a 1.3% branching ratio. Both reactions produce other gammas with much higher branching ratios. Measuring each group of wires at once reduces the measurements required for a foil package from ten to three. Group 1 of the wires for measuring is cobalt, tantalum,

manganese and aluminum; group 2 is indium, lanthanum and copper; and group 3 is nickel, vanadium and gold.

High Level Activation Measurements

To verify the foils' reactions of interest would activate at the designed levels they were irradiated in the rabbit tube of the OSU research reactor. The rabbit tube pneumatically locates the item for irradiation next to the core. The operator can manually insert and eject the item for irradiation or a timer can be used to eject automatically at the preset time. The rabbit tube's neutron energy spectrum from previous experimentation is shown in Figure 9.

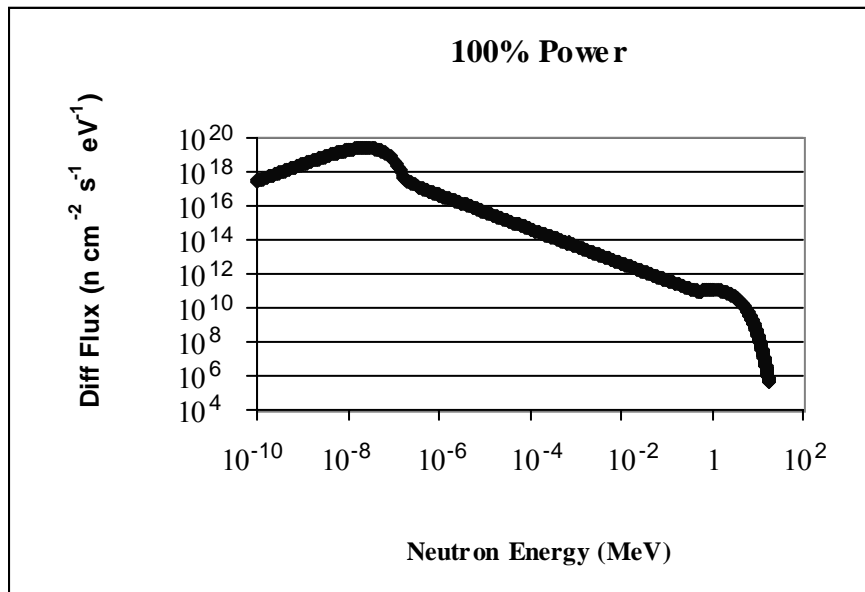


Figure 9. Differential flux in OSU rabbit tube.

The gold, aluminum, copper and manganese foils in a package were irradiated in the rabbit tube for 1000 seconds at 20% power to expose them to a fluence of 1.8×10^{14} n cm⁻² for fast and epithermal neutrons (over 0.5 eV). The indium, vanadium and nickel foils in a package were irradiated in the rabbit tube for 1000 seconds at 10%

power to expose them to a fluence of $9 \times 10^{13} \text{ n cm}^{-2}$. The foil packages were wrapped in cadmium to partially inhibit thermal activation so the packages could be safely handled when removing them from the rabbit tube. The results are tabulated in Table 7. The (n,α) reaction of copper the $(n,2n)$ reaction of manganese were not detected. These both have relatively long half-lives of 5.27 years and 312 days respectively. Gold was initially measured two days after irradiation and had so much activity that the dead time was at 98%. This was a product of the (n,γ) reaction and not the reaction of interest $(n,2n)$. The dead time was reduced to 25% by moving the foil 13 cm from the detector. Another count was made 19 days after irradiation and the dead time was down to 7% with the wire placed 1 mm from the face of the detector. The peak of interest $(n,2n)$ was also relatively larger than the shorter lived (n,γ) reaction.

Table 7. Rabbit tube activation results.

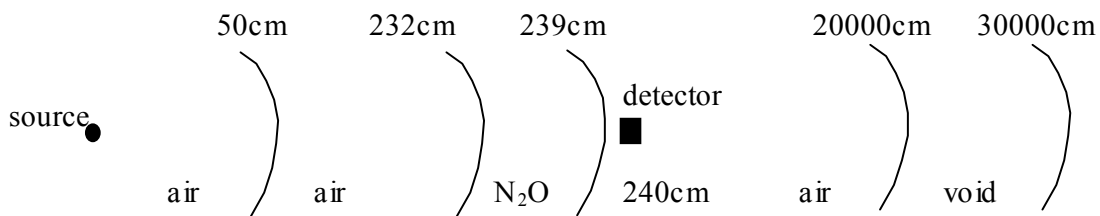
Element	ROI	$T_{1/2}$ (h)	Delay Time (h)	Measured Act (μCi)	Act at Activation (μCi)
Au	$n,2n$	148	475.77	3.04×10^{-5}	2.82×10^{-4}
Au	n,γ	64.685	475.77	1.35×10^{-1}	2.21×10^1
Al	n,α	14.95	43.05	2.45×10^{-7}	1.80×10^{-6}
Cu	n,α	46205	43.05	N/A	N/A
Cu	n,γ	12.701	43.05	1.12	1.18×10^1
Mn	$n,2n$	7490	43.05	N/A	N/A
Mn	n,γ	2.578	43.05	5.43×10^{-4}	5.78×10^1
In	n,n'	4.485	18.133	1.76×10^{-1}	2.90
In	n,γ	0.903	18.133	4.40×10^{-4}	4.88×10^2
V	n,α	43.7	18.133	3.17×10^{-5}	4.23×10^{-5}
Ni	$n,2n$	35.6	18.133	9.55×10^{-6}	1.36×10^{-5}
Ni	n,p	1701.1	18.133	7.60×10^{-3}	7.66×10^{-3}

V. Liquid Air Experiments

This chapter investigates the concept of using liquid to replicate large volumes of air. The investigation consisted of a simulation of the general concept, the design of a physical experiment, a simulation of the experiment, and the conduct of the experiment.

Liquid/Air Concept Simulation

The concept of using compressed gasses or liquids to represent distances of air was investigated using SCALE to simulate neutron transport through 7 cm of liquid N₂O as shown in Figure 10. A point source was modeled as monoenergetic (14 MeV) with a source magnification of 10¹⁵. All boundaries were modeled as spheres so nothing would affect the transport of neutrons through air except the liquid N₂O. A point detector was placed 240 cm from the source to measure the neutron flux after transporting through the liquid N₂O. To get neutron flux as the output of SCALE, the response function was set to one. The N₂O was modeled as 67% nitrogen, 33% oxygen with density of 1.53 g cm⁻³ [31]. The air was modeled as 78% nitrogen and 22% oxygen with a density of 1.1 mg cm⁻³.



Not to Scale

Figure 10. Nitrous oxide simulation.

The simulation was repeated by replacing the N₂O with liquid air modeled the same as the dry air but with density of 1.53 g cm⁻³. The simulation was again repeated replacing the N₂O with the modeled air and placing point detectors between 93 and 175 meters to measure the neutron flux after transporting through air.

Using the number of atoms per unit volume, 7 cm of N₂O should be equivalent to 96 meters of air. The results of the simulations, graphed in Figure 11 with the dispersion factor (Equation 14) applied to the N₂O and liquid air results, lead us to believe that it is not quite that simple. If the 7 cm of N₂O was equivalent to 96 meters of air for neutron transport, the results should have crossed at 96 meters on the graph.

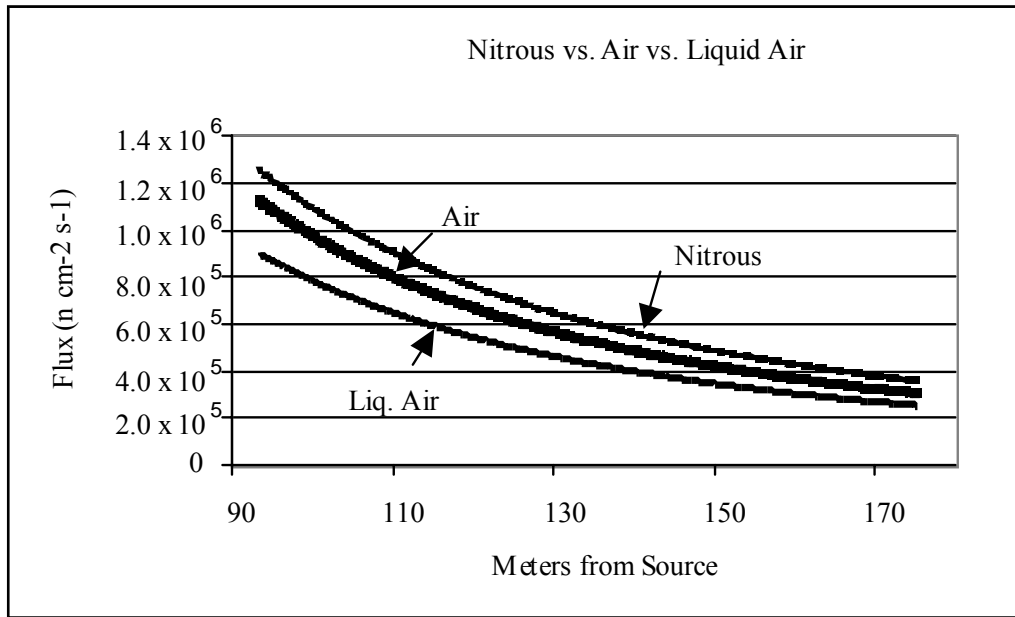


Figure 11. Comparison of SCALE simulations for N₂O, air and liquid air.

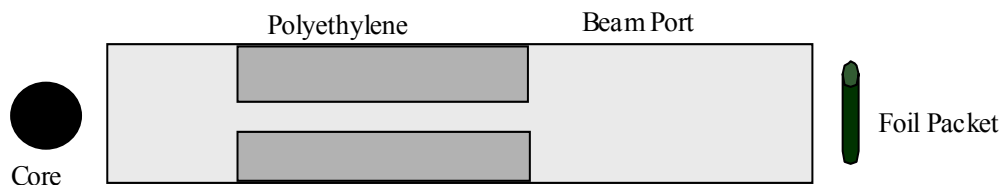
Liquid/Air Experiment Design

An experiment using the beam port of the OSU research reactor was designed with the original goal of sending foil activity measurements to ORNL by using N₂O to

simulate air over ground neutron transport while representing different volumes of air (e.g. 19 cm of N₂O in the cylinder represents 264 meters of air). Experiments and simulations were carried out concurrently and the results used to shape further experiments and simulations. The results of the liquid/air concept simulation changed the original goal and experiment to comparing activation results using N₂O to results without N₂O to determine an empirical fit. The foil activations would be accomplished in two consecutive reactor runs. The first run would be without N₂O with the foils located 21.5 cm inline and outside the end of the beam port. For the second run, the N₂O cylinder would be attached to the end of the beam port and the foils located 1.5 cm beyond the cylinder and inline with the beam port.

OSU's research reactor has the capability of producing a wide spectrum of neutrons as shown in Figure 9. The integral neutron flux near the core has been measured to be $2 \times 10^{12} \text{ n cm}^{-2} \text{ s}^{-1}$ and $10^8 \text{ n cm}^{-2} \text{ s}^{-1}$ at the outside end of the beam port at full power [26]. The reactor also has strict operating restrictions on the amount of radiation (2 mrem h^{-1}) that can escape the facility. The open beam port is an avenue for radiation that must be shielded to maintain safe levels of exposure.

Additionally, to replicate a nuclear detonation the source must appear as a point. Therefore, two polyethylene plugs, 30 cm each, with a 38 mm hole in the center were added to the beam port to collimate the source and make it appear as a point as shown in Figure 12.



Not To Scale

Figure 12. Collimated OSU source experiment.

The plugs were inserted 82.4 cm from the outside of the beam port to make the source appear as a point to the six inch opening at the end of the beam port. The method of using similar triangles was used to determine the distance of insertion required as shown in Figure 13.

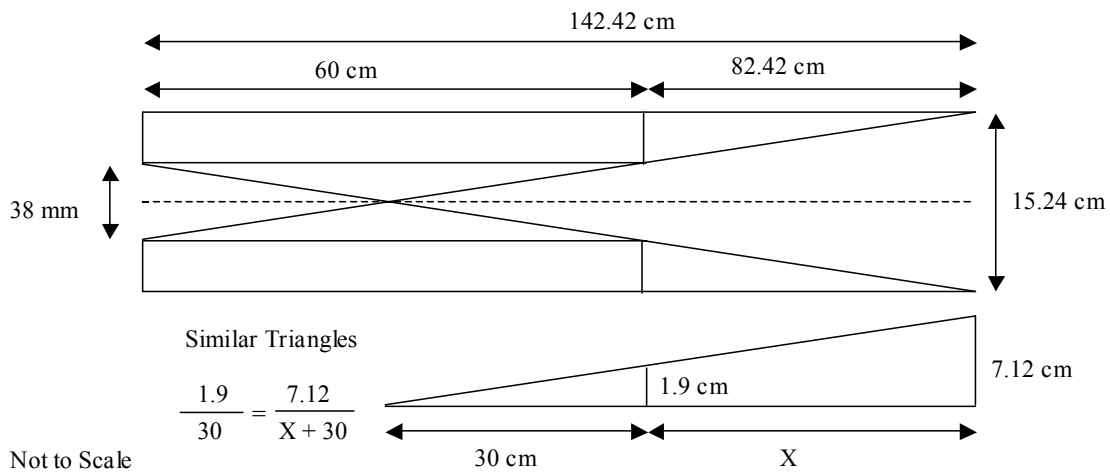


Figure 13. Collimating the OSU reactor to appear as a point source.

Cadmium was added to the outside end of the plugs and the beam port between the end of the plugs and the outside opening was lined with cadmium to prevent thermal neutrons from scattering back in. The hydrogen in the polyethylene (CH_2) and the Barytes cement containment structure slows the neutrons down by elastic scattering and the cadmium, with a huge thermal absorption cross-section, captures them.

Liquid/Air Experiment Simulation

The OSU research reactor beam port experiment was simulated using SCALE. The simulation was done using the geometry depicted in Figure 14. Experimental components were then added as needed to simulate individual experiments.

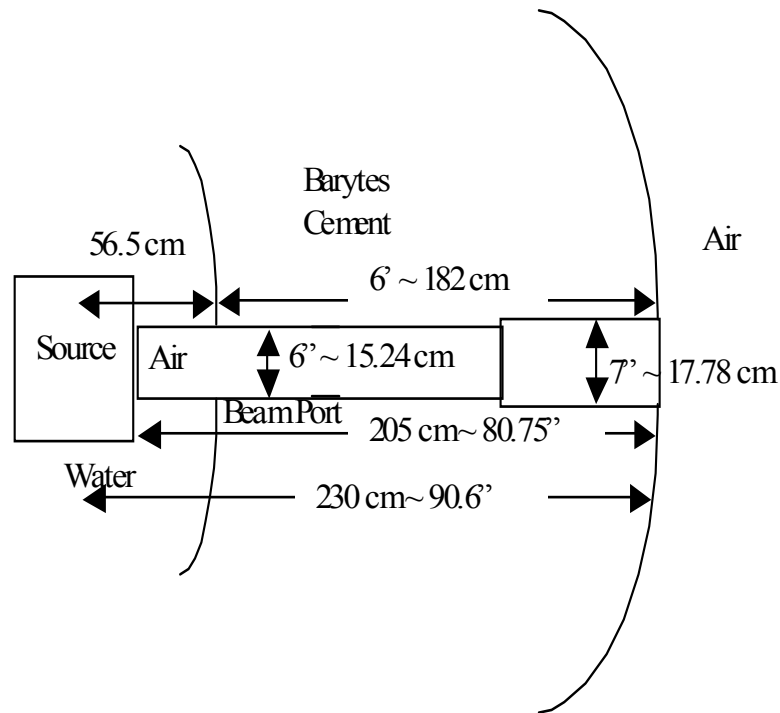


Figure 14. OSU reactor beam port simulation geometry.

The source was modeled as a 48 cm cube surrounded by water. The inner wall of the cement containment model was modeled as a sphere 56.5 cm from the center of the core. The outer wall was modeled as a sphere 230 cm from the center of the core. The cement was modeled with a density of 3.3 g cm^{-3} corresponding with Barytes concrete [28]. The beam port was modeled as a right circular cylinder consisting of two parts with different diameters. The part closest to the core started 1 cm from the core, extended 159 cm horizontally and had a radius of 7.62 cm. The outside portion began

where the first part ended (184 cm from center of core) and extended to the outside of the cement containment structure (46 cm). The air in the beam port and outside the cement containment structure was modeled as 78% nitrogen and 22% oxygen with a density of 1.1 mg/cm^3 . Point detectors were centered in the beam port 1 cm from the end closest to the core, 1 cm outside the end of the beam port and 21.5 cm off the end of the beam port where the foils would be placed. The response function was set to one so that the output of SCALE would be the flux. The source spectrum used was from previous experimental data taken in the central irradiation facility (CIF) located in the center of the core [10]. The source multiplication factor was 3.36×10^{16} and was determined by trial and error to get the integral flux at the end of the beam port closest to the reactor core to $3.6 \times 10^{12} \text{ n cm}^{-2} \text{ s}^{-1} \pm 19.5\%$, corresponding to previous experimental data taken from the rabbit tube [29].

The neutron flux from the simulation at 21.5 cm outside the beam port, the foil placement point, was $1.903 \times 10^9 \text{ n cm}^{-2} \text{ s}^{-1} \pm 17.2\%$. Using this result and operating at 450 kW, it would require about an hour and a half to reach a fluence of $10^{13} \text{ n cm}^{-2}$ and over 14 hours for $10^{14} \text{ n cm}^{-2}$. This simulation's resulting neutron flux was an order of magnitude higher than what had been previously measured.

Unsafe levels of gamma and neutron radiation were measured in the reactor building upon experimentation with the collimating polyethylene plugs. Because of this, all further beam port simulations replaced the collimating polyethylene plugs with a solid polyethylene plug 45 cm long in the outside end of the beam port to replicate actual experiments.

Keeping all parameters the same and exchanging the collimating polyethylene plugs with the solid plug at the end of the beam port gave a simulated neutron flux at the foil locations of $1.4625 \times 10^4 \text{ n cm}^{-2} \text{ s}^{-1} \pm 17.2\%$. This flux was five orders of magnitude less than the flux from the simulation with the collimating polyethylene plugs and should result in a safe level of radiation in the reactor building.

The effects of nitrous oxide were simulated using an N_2O container simulated by a right circular cylinder of 4130 steel with sidewalls of 0.5 cm [32]. The cylinder was 20 cm in diameter and 51 cm high. It was placed perpendicular against the end of the beam port so the outside edge was 250 cm from the center of the core. The detector was placed 1.5 cm from the cylinder centered on the beam port or 251.5 cm from the center of the core as shown in Figure 15. The 4130 steel was modeled as in Table 8. The N_2O was modeled as 67% nitrogen, 33% oxygen with density of 1.53 g cm^{-3} . The resulting flux at the foil location was $2.2041 \times 10^3 \text{ n cm}^{-2} \text{ s}^{-1} \pm 17.5\%$.

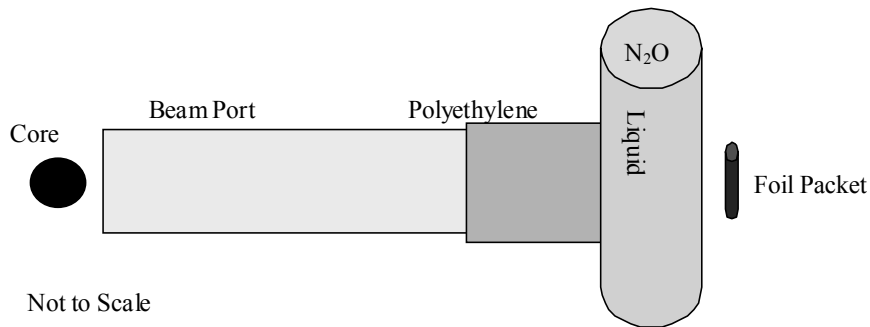


Figure 15. OSU beam port characterization with poly plug and N_2O .

Table 8. 4130 steel composition [9].

Element	Percentage
Iron	97.56
Carbon	0.30
Manganese	0.65
Phosphorus	0.04
Sulfur	0.05
Silicon	0.25
Chromium	0.95
Molybdenum	0.20

This flux was too low to activate any of the reactions of interest for AFIDS to measurable amounts but should be enough to activate the (n,γ) reactions of gold and copper to characterize the neutron spectrum if the escaping radiation could be controlled enough to allow a high power lengthy run. This spectrum could then be compared to the spectrum obtained from the run without the N_2O to get more insight on the effect of N_2O on neutron transport.

Experiment

Characterization of neutron spectra is done at the OSU research reactor using the SAND-II program. The SAND-II program determines neutron spectra by multiple foil integration using the iterative method and generates a 620-group neutron energy spectrum. The required inputs are the saturation activity per nucleus of the characterization foils used. The characterization foils used at the OSU research reactor consisted of gold, cobalt and copper in two sets. One set was wrapped in cadmium and the other was bare. The spreadsheet in Table 9 was created for calculating the saturation activity per nucleus.

Table 9. SAND-II input calculations.

wire/foil	* mass (mg)	% abund.	AW (g/mol)	Target Nuclei	Isotope of Interest	* Activity (dps)	T ^{1/2} (m)	λ (m ⁻¹)	* Time Irradiated (m)	Saturated Activity (dps/nucleus)
Bare										
Au	8.99	100	196.97	2.75 x 10 ¹⁹	¹⁹⁸ Au	110.59	3881.09	0.00018	15	1.50 x 10 ⁻¹⁵
Co	1	100	58.93	1.02 x 10 ¹⁹	⁶⁰ Co	100	2772276	2.5 x 10 ⁻⁷	15	2.61 x 10 ⁻¹²
Cu	1	69.17	62.93	9.57 x 10 ¹⁸	⁶⁴ Cu	100	762.06	0.00091	15	7.71 x 10 ⁻¹⁶
Fe	1	0.282	57.93	1.04 x 10 ¹⁹	⁵⁹ Fe	100	64080	1.1 x 10 ⁻⁵	15	5.93 x 10 ⁻¹⁴
Cd covered										
Au	1	100	196.97	3.06 x 10 ¹⁸	¹⁹⁸ Au	100	3881.09	0.00018	15	1.22 x 10 ⁻¹⁴
Co	1	100	58.93	1.02 x 10 ¹⁹	⁶⁰ Co	100	2772276	2.5 x 10 ⁻⁷	15	2.61 x 10 ⁻¹²
Cu	1	69.17	62.93	9.57 x 10 ¹⁸	⁶⁴ Cu	100	762.06	0.00091	15	7.71 x 10 ⁻¹⁶
Fe	1	0.282	57.93	1.04 x 10 ¹⁹	⁵⁹ Fe	100	64080	1.1 x 10 ⁻⁵	15	5.93 x 10 ⁻¹⁴

* Required inputs

Isotope data from Chart of the Nuclides, 16th Ed.

The first experiment conducted at the OSU research reactor for this thesis was to characterize the flux at the end of the beam port with the collimation apparatus of polyethylene plugs and cadmium shielding installed as shown in Figure 12. The outside of the beam port was shielded with lead, cadmium and boronated bricks. The foils were located 21.5 cm outside the beam port as shown in Figure 16. The reactor was brought up to 20% power (100 kW) and radiation surveys conducted to ensure regulatory compliance and safety. The escaping neutron and gamma radiation in the reactor building was approximately 60 mrem/h, high enough that the run was shut down after only 15 minutes. For this experiment, only three foils were used as inputs to the SAND-II program, both gold foils and the bare copper. The rest did not have measurable activity. The generated spectrum is shown in Figure 17. It is interesting to see the impact the polyethylene and cadmium have when comparing this spectrum to the rabbit

tube spectrum in Figure 9. The polyethylene has smoothed the spectrum while thermal neutron attenuation is evident from the cadmium and divergence by a factor of eight.



Figure 16. Characterization foils at end of beam port.

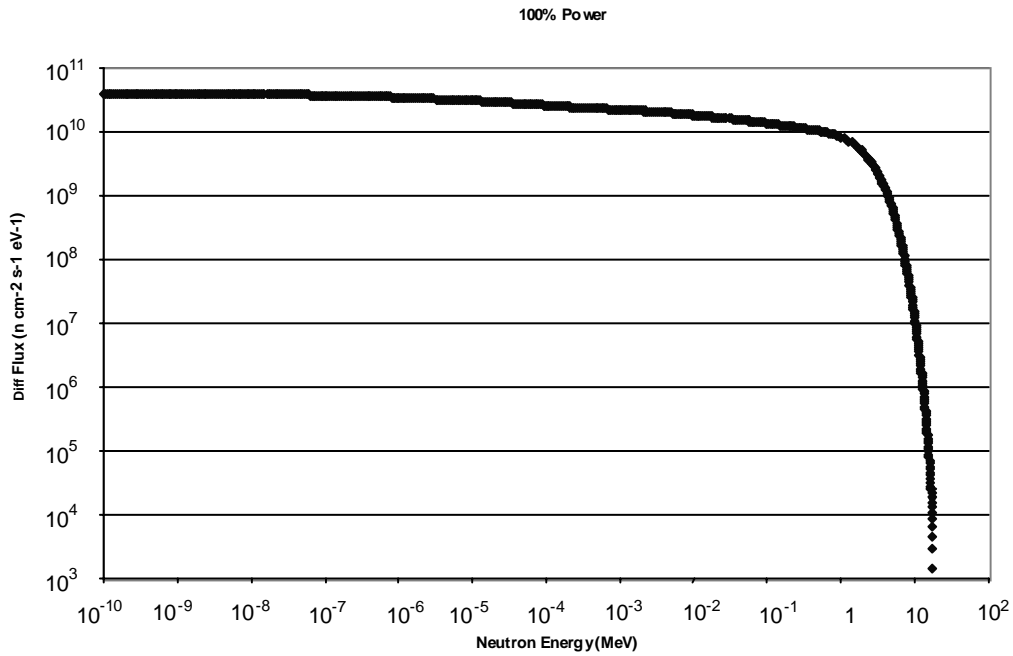


Figure 17. Neutron energy spectrum at end of OSU collimated beam port.

Continued operation could not safely be maintained at a high enough power in this configuration to produce a flux capable of activating the foils for further experimentation, to include a run using N₂O. Massive shielding had been applied but the escaping radiation was still too large.

In order to minimize escaping radiation while maintaining maximum flux, a polyethylene plug was placed in the outside 45 cm of the beam port as shown in Figure 15. The plug would thermalize neutrons that could then be captured by the cadmium and boronated bricks shielding the outside of the beam port. Lead would scatter the gammas.

Characterization foils were located 21.5 cm from the beam port. Shielding was built up from the floor and from the viewpoint of the radiation coming out of the beam port consisted of a cadmium layer followed by a layer of lead and a layer of boronated bricks as shown in Figure 18. The reactor was brought up to 10% power and radiation surveys begun. The gamma levels were quite low but the neutron levels were extremely high (e.g. 600 mrem/h) all around the beam port so the run was terminated after 15 minutes of operation. Both gold characterization foils had enough activation to be counted but also had error quoted at two sigma of 14-17%. Their calculated saturated activities per nucleus were input into SAND-II and a piecemeal spectrum came out. The integral neutron flux was approximately $10^5 \text{ n cm}^{-2} \text{ s}^{-1}$, seven times the flux from the simulation.



Figure 18. Shielding on end of OSU beam port.

The results of the previous experiment were not known when the nitrous bottle was placed on the end of the beam port and the foils placed 1.5 cm from the cylinder as shown in Figure 19. The shielding was supplemented by hanging sheets of cadmium over the outside of the shielding to absorb thermal neutrons. The reactor was brought up to only 5% power initially so safety surveys could be conducted. Again, the neutron levels were unsafe and the reactor was shut down after only a few minutes of operation. The neutron levels were approximately 600 mrem/h near the containment structure all around the beam port but declined to approximately 300 mrem/h behind the shielding. It was postulated that the polyethylene plug was scattering the fast and epithermal neutrons out into the concrete containment structure where they were getting further scattered out of the wall and into the room. This, in effect, made the entire wall a source. The shielding was effective but only covered the beam port opening. This was not observed during the simulation as the shielding outside the beam port was not modeled and no detectors were placed beyond the foil location.



Figure 19. N₂O in place at end of OSU beam port.

The gold characterization foils were the only ones that had enough activity to be counted. The foils were counted for approximately 39 hours to minimize error but the activity in the bare foil was 0.0472 disintegrations per second with 25.15% error at two sigma and the cadmium-covered foil had 0.0304 disintegrations per second with 44.29% error. The saturated activity per nucleon was two orders of magnitude lower than previous activities when calculated for SAND-II input. SAND-II did converge but the resulting spectrum was, not surprisingly, again piecemeal. The flux was $1.7 \times 10^3 \text{ n cm}^{-2} \text{ s}^{-1}$, two orders of magnitude less than without the N₂O and in the same range as the simulation. These results have too much error associated with them to make definitive comparisons but the effect of the N₂O in the steel cylinder decreasing flux is readily observed.

VI. Conclusions and Recommendations

Conclusions

The only true validation of the methodology at ORNL is to conduct an outside test as using N_2O to replicate large volumes of air did not give results to send to ORNL. An outside test allows air over ground transport of neutrons, complete and measurable activation of foils, ability to conduct spectroscopy of the foils, and an independent and valid set of data to transfer to ORNL for validation.

SCALE can be very complex. Accuracy can be improved if care and time are taken to replicate the geometry and materials involved as precisely as possible. The initial simulations of the neutron flux at the outer end of the OSU reactor beam port were off by a factor of nearly one thousand. Simulating the core as a cube instead of a point, using more accurate geometry, and better simulation of the reactor materials brought the simulated neutron flux to within a factor of seven of the measured neutron flux. More precise simulation of the actual core and further refinement of the geometry and material should produce results that are even more accurate.

Only a small portion of the SCALE program was used in this thesis. The SAS4 module was used so the modeling could be in 3-D. It is not very easy to learn but the interactive input makes it easy to operate.

Neutron induced reactions in gold and cobalt that were not originally considered could be of use. The (n,γ) thermal reaction of gold is very sensitive and has a 2.69 day half-life. Cobalt has an $(n,2n)$ reaction with a threshold of 10.6 MeV and a half-life of 71 days. The (n,p) reaction of cobalt has a threshold of 0.8 MeV and a half-life of 44.5 days.

It only makes sense to include these reactions since the spectroscopy will be done anyway.

The error associated with the activity measurements of the foils must be minimized. The use of wires does not significantly reduce the accuracy as the difference in solid angle between a point and a wire was shown to be negligible for the spectroscopy system used. The importance of a good calibration was driven home as initial results had over 50% error. Time and resources will be at a premium immediately following a domestic nuclear event and it was shown that the foils could be measured in three groups to maximize these resources. However, caution must be used when measuring the gold as the massive activity can saturate the system resulting in high dead time. Some foils, such as indium, require some cooling time so the reactions of interest can be more readily detected.

Using N_2O or liquid air to simulate large volumes of air is a very attractive proposition however the concept is not as simple as first thought. A possible explanation is that the angle of approach between neutrons and nucleons is different at different distances from the source [20]. This would change the probability of interaction and add an unknown factor to the solution. For example, point A in air in Figure 20 has a corresponding point B in N_2O . Point A would have a different probability of interacting with a neutron leaving the source at a specific angle than would Point B. The problem of different angles of interaction at depth needs to be resolved.

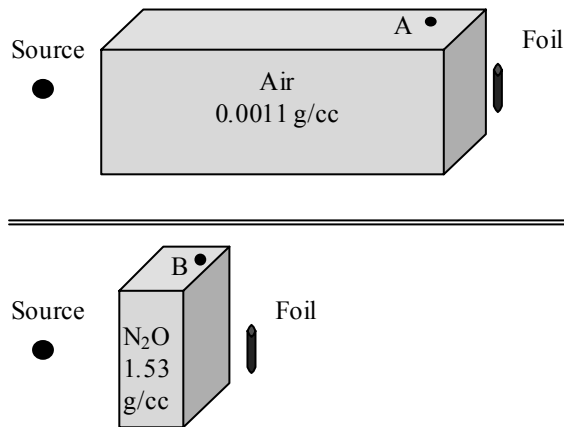


Figure 20. N₂O and air “equivalency”.

The OSU research reactor has many capabilities. Irradiating experiments on the outside of the beam port is not currently one of them. The beam port points directly toward administrative offices and limits configuration based upon safety. Shielding has to be moved into place once the experiment is set up and then removed to access the experiment. This can be very time consuming and also increase exposure to dangerous levels. The escaping radiation is a safety concern, especially when the items in the outer end of the beam port scatter neutrons into the cement containment structure and then into the room. A substantial shielding plan is required for even the most basic operations.

Recommendations

The use of the OSU reactor beam port should be enhanced. Easy-to-use shielding should be designed to seal around the open beam port and contain escaping radiation. One idea is to fabricate a tank that seals around the port leaving a cavity for experiments. The tank could then be filled with ionized water that is available at OSU to provide a moderator for the neutrons. Once slowed down, the neutrons could be captured by

cadmium sheets. Another idea is to build shielding on a pallet-type jack. The shielding could then be raised and lowered hydraulically.

I would not recommend pursuing the use of N_2O or liquid air at OSU unless it could be placed inside the beam port. Obtaining approval to place pressurized containers in the beam port where they are subject to heating would be difficult. Results would be better if the foils are located far enough away from the N_2O so that the neutrons coming through the N_2O appear as from a point source. This requires space and shielding along the complete path between the N_2O and the foil to keep neutrons from scattering in from leakage around the N_2O . OSU does not have much space and the shielding would have to contend with gammas as well as neutrons. On the other hand, if a facility with a dedicated experimentation room was available, pursuing N_2O or liquid air use could be very beneficial. The shielding between the N_2O and the foils would only have to be for thermal neutrons and backscatter onto the foil would be minimized. A fabricated container built specifically for the experimentation area could be sized for whatever depth is desired. The requirement for shielding between the N_2O and foils might even be able to be done away with if the container was designed to not have any leakage around it.

Testing the foils with an outside shot to get results to send to ORNL for methodology verification is the best follow-on research for this project. It could include more options for wire choice. Gold, vanadium and cobalt are all rather expensive. Other wire options in the epithermal range to better cover the spectrum could also be researched. Design and testing of a package for the foils could be researched, especially

if they are going to production. If outside shots become available, or areas with more room to work with, research on using N₂O or liquid air could be beneficial.

Appendix A. Pu-Be Source

This thesis used a plutonium-beryllium (Pu-Be) source. A Pu-Be source generates the majority of its neutrons from (α, n) reactions with some contribution from Be($n, 2n$) and Pu(n, f). Another small contributor is the inelastic scattering of alpha particles by the beryllium that yields low energy neutrons [2]. A Pu-Be source initially has an increasing neutron yield due to small quantities of ^{241}Pu in the source. Plutonium-241 is a beta emitter that decays to ^{241}Am . Americium-241 is an alpha emitter which generates more (α, n) reactions resulting in more neutrons. After several decades, the ^{241}Am reaches a maximum and gradually starts to decline.

The total yield of a stable source at any time is derived by M. Edward Anderson of Mound Laboratory in a 1968 Nuclear Applications article [1]. It is given as

$$Q(t) = Q(0) \left\{ 1 + \frac{a_4}{a_1} \frac{\lambda_4 \lambda_3 N_3}{(\lambda_1 N_1 + \lambda_2 N_2)(\lambda_3 - \lambda_4)} (e^{-\lambda_4 t} - e^{-\lambda_3 t}) \right\} \quad (15)$$

where

$$Q(0) = a_1 \lambda_1 N_1 + a_2 \lambda_2 N_2. \quad (16)$$

The time prior to source fabrication when the americium that was formed during the birth of the plutonium is separated from the plutonium is designated as $t = 0$. The average neutron yield per alpha particle is a , λ is the disintegration constant and N is the number of atoms present at time $t = 0$. The subscript 1 corresponds to ^{239}Pu , 2 to ^{240}Pu , 3 to ^{241}Pu and 4 to ^{241}Am . Since the alpha particle energies of ^{239}Pu and ^{240}Pu are almost identical, $a_1 \approx a_2$, and

$$Q(0) \approx a_1 (\lambda_1 N_1 + \lambda_2 N_2). \quad (17)$$

The value of a_1 is not known but the yield at the time of the source fabrication ($Q(t_1)$) is typically known from the source documentation. Using this we can solve for

$$Q(0) = \frac{Q(t_1)}{1 + \frac{a_4}{a_1} \frac{\lambda_4 \lambda_3 N_3}{(\lambda_1 N_1 + \lambda_2 N_2)(\lambda_3 - \lambda_4)} (e^{-\lambda_4 t_1} - e^{-\lambda_3 t_1})} \quad (18)$$

and then solve for $Q(t)$ using Equation 15. The value of $\frac{a_4}{a_1}$ is 1.23 ± 0.05 by experimentation.

The Pu-Be source used in this experiment, M-1170 produced at Mound Laboratory, had an initial neutron emission rate ($Q(t_1)$) of $9.04 \times 10^6 \text{ n s}^{-1}$ on 9 March 1962 [16]. It was composed of 39.28 g of beryllium and 76.36 g of plutonium. The composition of the plutonium can be inferred from Anderson's article to be 93.4% ^{239}Pu , 6.1% ^{240}Pu and 0.55% ^{241}Pu with a birth date (t_0) of 25 April 1961. All this information along with half-lives was used to create the spreadsheet in Table 10. Equation 13 was implemented to calculate the number of atoms. Once the information is set up, Equation 18 and Equation 15 are solved to give the yield as of the date input by the user (t). To check the validity of the calculations, the yield for 22 October 1987 was calculated. It was $1.09 \times 10^7 \text{ n s}^{-1}$, within 1.9% of Whitworth's experimental value of $1.07 \times 10^7 \text{ n s}^{-1} \pm 3\%$ for the same source [33].

Table 10. M-1170 Pu-Be source calculator.

Calculations to determine activity of M-1170 Pu-Be source.

N1 =	1.79706 x 10 ²³	t0 =	4/25/1961	
N2 =	1.16878 x 10 ²²	t1 = (yr)	3/9/1962	0.871233
N3 =	1.04944 x 10 ²¹	t = (yr)	10/22/2004	43.52329
λ1 = (/yr)	2.84077 x 10 ⁻⁵			
λ2 = (/yr)	0.000105022	Q(t1) = (n/s)	9.04 x 10 ⁶	
λ3 = (/yr)	0.05251115			
λ4 = (/yr)	0.001513422			
Q(t0) = (n/s)	8917066.151			
Q(t) = (n/s)	11280868.71			

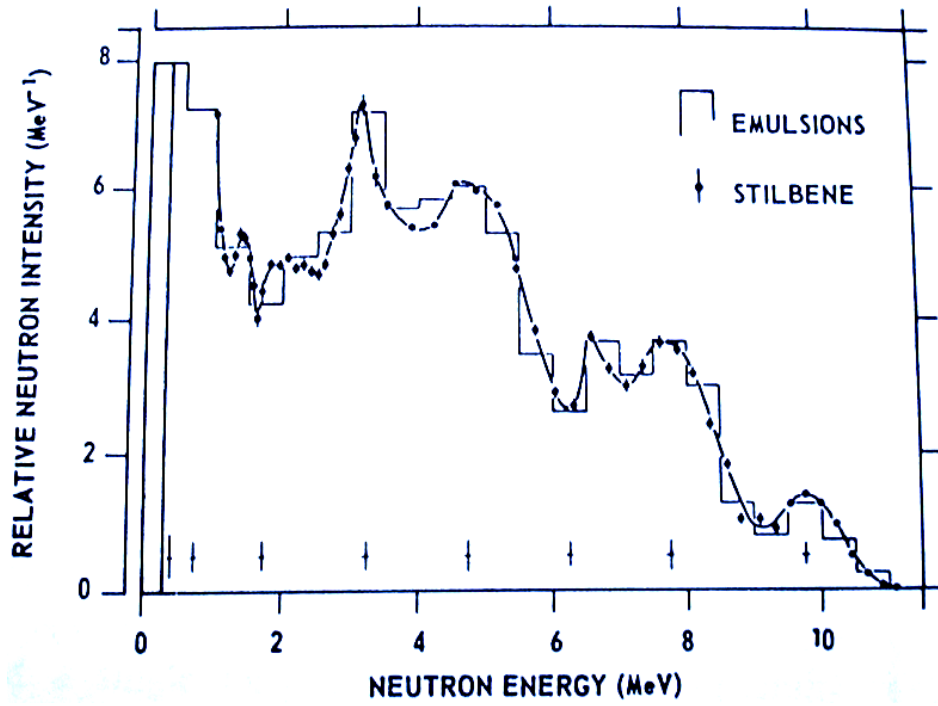
Change the date in E5 to get the Q(t) of that date.

Based on M. Edward Anderson's article, "Increases in Neutron Yields of Plutonium-Beryllium (α ,n) Sources"

Nuclear Applications, Volume 4, March 1968

The Pu-Be source is contained in a barrel of paraffin as shown in Figure 7. The paraffin is approximately 5 inches thick and the source is approximately 21.5 cm from the end of the barrel. The yield on 22 October 2004 when irradiation was conducted was calculated to be $1.128 \times 10^7 \text{ n s}^{-1}$. Using the theory behind Equation 1, the flux at the mouth of the barrel was $1.9 \times 10^3 \text{ n cm}^{-2} \text{ s}^{-1}$ and a 15-hour irradiation gave a fluence on the order of $1 \times 10^8 \text{ n cm}^{-2}$ not accounting for any decay during the activation.

Neutron energy spectra vary among different Pu-Be sources. It has been shown that generally larger sources have a higher percentage of 0-3 MeV neutrons [2]. Sources at Mound Laboratory contained between 1 and 160 g of plutonium. Source M-1170 contained 76.36 g. A spectrum for an 80 g source is shown in Figure 21.



Source: Anderson, Nuclear Instruments and Methods, 1972

Figure 21. 80 g Pu-Be source neutron energy spectrum.

Appendix B. Gammas from Common Neutron Reactions

Table 11 contains a list of common neutron initiated reactions for the foils selected for this thesis. It lists the percentage of the naturally occurring isotope, mode of decay, percentage of decay, the energy of the resulting gamma rays and their associated branching ratio [17]. This data can then be sorted by gamma energy to screen for gammas that are similar in energy and might cause summing problems during counting. A feeling of the magnitude of the summing problem can be gained by looking at the half-life, percentage of natural occurrence, the percentage of decay and the branching ratio [3].

The indented reactions are secondary reactions or reactions of daughters. The results of the 15-hour Pu-Be are listed and whether or not the reaction is one of the AFIDS reactions of interest.

Table 11. Common gammas from selected foils.

Reaction	T _{1/2}	% natural	Decay	% Decay	γ energy [keV]	branching %	Visible with Pu-Be	ROI
²⁷ Al(n,γ) ²⁸ Al	2.25m	100	β-	100	1778.85	100	N	N
²⁷ Al(n,2n) ²⁶ Al	7.1 x 10 ⁵ y	100	ε	100	1129.67	2.5	N	N
²⁷ Al(n,2n) ²⁶ Al	7.1 x 10 ⁵ y	100	ε	100	1808.65	99.76	N	N
²⁷ Al(n,p) ²⁷ Mg	9.45m	100	β-	100	843.76	71.8	N	N
²⁷ Al(n,p) ²⁷ Mg	9.45m	100	β-	100	1014.44	28	N	N
²⁷ Al(n,α) ²⁴ Na	14.95h	100	β-	100	1368.633	100	N	Y
²⁷ Al(n,α) ²⁴ Na	14.95h	100	β-	100	2754.028	99.944	N	Y
¹⁹⁷ Au(n,γ) ¹⁹⁸ Au	2.6952d	100	β-	100	411.802	95.58	Y	N
¹⁹⁷ Au(n,γ) ¹⁹⁸ Au ^m	2.27d	100	IT	100	97.21	69.3	N	N
¹⁹⁷ Au(n,γ) ¹⁹⁸ Au ^m	2.27d	100	IT	100	180.31	50	N	N
¹⁹⁷ Au(n,γ) ¹⁹⁸ Au ^m	2.27d	100	IT	100	204.1	40.8	N	N
¹⁹⁷ Au(n,γ) ¹⁹⁸ Au ^m	2.27d	100	IT	100	214.89	77	N	N
¹⁹⁷ Au(n,γ) ¹⁹⁸ Au ^m	2.27d	100	IT	100	333.82	17	N	N
¹⁹⁷ Au(n,2n) ¹⁹⁶ Au	6.167d	100	β-	7.2	426.1	6.6	N	Y
¹⁹⁷ Au(n,2n) ¹⁹⁶ Au	6.167d	100	ε	92.8	333.03	22.9	N	Y
¹⁹⁷ Au(n,2n) ¹⁹⁶ Au	6.167d	100	ε	92.8	355.73	87	N	Y
¹⁹⁷ Au(n,2n) ¹⁹⁶ Au ^m	9.6h	100	IT	100	137.69	1.3	N	Y
¹⁹⁷ Au(n,2n) ¹⁹⁶ Au ^m	9.6h	100	IT	100	147.81	43	N	Y
¹⁹⁷ Au(n,2n) ¹⁹⁶ Au ^m	9.6h	100	IT	100	168.37	7.7	N	Y
¹⁹⁷ Au(n,2n) ¹⁹⁶ Au ^m	9.6h	100	IT	100	188.27	37	N	Y
¹⁹⁷ Au(n,2n) ¹⁹⁶ Au ^m	9.6h	100	IT	100	285.49	4.3	N	Y
¹⁹⁷ Au(n,2n) ¹⁹⁶ Au ^m	9.6h	100	IT	100	316.19	2.9	N	Y
¹⁹⁷ Au(n,p) ¹⁹⁷ Pt	19.96h	100	β-	100	77.35	17	N	N
¹⁹⁷ Au(n,p) ¹⁹⁷ Pt	19.96h	100	β-	100	191.437	3.7	N	N
¹⁹⁷ Au(n,p) ¹⁹⁷ Pt ^m	1.59h	100	β-	3.3	279	2.4	N	N
¹⁹⁷ Au(n,p) ¹⁹⁷ Pt ^m	1.59h	100	IT	96.7	346.5	11.1	N	N
¹⁹⁷ Au(n,α) ¹⁹⁴ Ir	19.3h	100	β-	100	293.541	2.5	N	N
¹⁹⁷ Au(n,α) ¹⁹⁴ Ir	19.3h	100	β-	100	328.448	13.1	N	N
¹⁹⁷ Au(n,α) ¹⁹⁴ Ir	19.3h	100	β-	100	645.146	1.18	N	N
¹⁹⁷ Au(n,α) ¹⁹⁴ Ir ^m	171d	100	IT	100	84.288	4.6	N	N
¹⁹⁷ Au(n,α) ¹⁹⁴ Ir ^m	171d	100	IT	100	112.23	8.3	N	N
¹⁹⁷ Au(n,α) ¹⁹⁴ Ir ^m	171d	100	β-	100	111.7	8.9	N	N
¹⁹⁷ Au(n,α) ¹⁹⁴ Ir ^m	171d	100	β-	100	324	2	N	N
¹⁹⁷ Au(n,α) ¹⁹⁴ Ir ^m	171d	100	β-	100	328.5	93	N	N
¹⁹⁷ Au(n,α) ¹⁹⁴ Ir ^m	171d	100	β-	100	338.8	55	N	N
¹⁹⁷ Au(n,α) ¹⁹⁴ Ir ^m	171d	100	β-	100	390.8	35	N	N

Reaction	T _{1/2}	% natural	Decay	% Decay	γ energy [keV]	branching %	Visible with Pu-Be	ROI
¹⁹⁷ Au(n,α) ¹⁹⁴ Ir ^m	171d	100	β-	100	482.6	97	N	N
¹⁹⁷ Au(n,α) ¹⁹⁴ Ir ^m	171d	100	β-	100	562.4	70	N	N
¹⁹⁷ Au(n,α) ¹⁹⁴ Ir ^m	171d	100	β-	100	600.5	62	N	N
¹⁹⁷ Au(n,α) ¹⁹⁴ Ir ^m	171d	100	β-	100	687.8	59	N	N
¹⁹⁷ Au(n,α) ¹⁹⁴ Ir ^m	171d	100	β-	100	1011.8	3.6	N	N
⁵⁹ Co(n,γ) ⁶⁰ Co	5.271y	100	β-	100	1173.228	99.85	N	Y
⁵⁹ Co(n,γ) ⁶⁰ Co	5.271y	100	β-	100	1332.492	99.9826	N	Y
⁵⁹ Co(n,2n) ⁵⁸ Co	70.88d	100	ε	100	810.7593	99.45	N	N
⁵⁹ Co(n,p) ⁵⁹ Fe	44.5d	100	β-	100	142.651	1.02	N	N
⁵⁹ Co(n,p) ⁵⁹ Fe	44.5d	100	β-	100	192.343	3.08	N	N
⁵⁹ Co(n,p) ⁵⁹ Fe	44.5d	100	β-	100	1099.245	56.5	N	N
⁵⁹ Co(n,p) ⁵⁹ Fe	44.5d	100	β-	100	1291.59	43.2	N	N
⁵⁹ Co(n,α) ⁵⁶ Mn	2.578h	100	β-	100	846.754	98.9	N	N
⁵⁹ Co(n,α) ⁵⁶ Mn	2.578h	100	β-	100	1810.72	27.2	N	N
⁵⁹ Co(n,α) ⁵⁶ Mn	2.578h	100	β-	100	2113.05	14.3	N	N
¹¹⁵ In(n,n') ¹¹⁵ In	4.485h	95.71	IT	95	336.241	45.8	N	Y
¹¹⁵ In(n,γ) ¹¹⁶ In ^m	54.2m	95.71	β-	100	138.326	3.29	N	N
¹¹⁵ In(n,γ) ¹¹⁶ In ^m	54.2m	95.71	β-	100	416.86	27.7	Y	N
¹¹⁵ In(n,γ) ¹¹⁶ In ^m	54.2m	95.71	β-	100	818.7	11.5	Y	N
¹¹⁵ In(n,γ) ¹¹⁶ In ^m	54.2m	95.71	β-	100	1097.3	56.2	Y	N
¹¹⁵ In(n,γ) ¹¹⁶ In ^m	54.2m	95.71	β-	100	1293.54	84.4	Y	N
¹¹⁵ In(n,γ) ¹¹⁶ In ^m	54.2m	95.71	β-	100	1507.4	10	Y	N
¹¹⁵ In(n,γ) ¹¹⁶ In ^m	54.2m	95.71	β-	100	1753.8	2.46	N	N
¹¹⁵ In(n,γ) ¹¹⁶ In ^m	54.2m	95.71	β-	100	2112.1	15.5	Y	N
¹¹⁵ In(n,2n) ¹¹⁴ In	1.198m	95.71	all					N
¹¹⁵ In(n,p) ¹¹⁵ Cd	2.228d	95.71	β-	100	260.896	1.94	N	N
¹¹⁵ In(n,p) ¹¹⁵ Cd	2.228d	95.71	β-	100	336.241	45.9	N	N
¹¹⁵ In(n,p) ¹¹⁵ Cd	2.228d	95.71	β-	100	492.351	8.03	N	N
¹¹⁵ In(n,p) ¹¹⁵ Cd	2.228d	95.71	β-	100	527.901	27.5	N	N
¹¹⁵ In(n,α) ¹¹² Ag	3.13h	95.71	β-	100	606.7	3.1	N	N
¹¹⁵ In(n,α) ¹¹² Ag	3.13h	95.71	β-	100	617.4	43	N	N
¹¹⁵ In(n,α) ¹¹² Ag	3.13h	95.71	β-	100	692.7	1.08	N	N
¹¹⁵ In(n,α) ¹¹² Ag	3.13h	95.71	β-	100	694.8	3	N	N
¹¹⁵ In(n,α) ¹¹² Ag	3.13h	95.71	β-	100	851.2	1.03	N	N
¹¹⁵ In(n,α) ¹¹² Ag	3.13h	95.71	β-	100	1312.3	1.2	N	N
¹¹⁵ In(n,α) ¹¹² Ag	3.13h	95.71	β-	100	1387.7	5.4	N	N

Reaction	T _{1/2}	% natural	Decay	% Decay	γ energy [keV]	branching %	Visible with Pu-Be	ROI
¹¹⁵ In(n,α) ¹¹² Ag	3.13h	95.71	β-	100	1613.6	2.8	N	N
¹¹⁵ In(n,α) ¹¹² Ag	3.13h	95.71	β-	100	2106.2	2.4	N	N
¹¹⁵ In(n,α) ¹¹² Ag	3.13h	95.71	β-	100	2506.8	1.08	N	N
¹¹³ In(n,γ) ¹¹⁴ In	1.198m	4.29	all					N
¹¹³ In(n,2n) ¹¹² In	14.4m	4.29	ε	56	606.4	1.11	N	N
¹¹³ In(n,2n) ¹¹² In	14.4m	4.29	ε	56	617.1	4.6	N	N
¹¹³ In(n,2n) ¹¹² In ^m	20.8m	4.29	IT	100	156.4	13.2	N	N
¹¹³ In(n,p) ¹¹³ Cd	7.7 x 10 ¹⁵ y	4.29	all					N
¹¹³ In(n,α) ¹¹⁰ Ag	24.6s	4.29	β-	99.7	657.5	4.5	N	N
¹¹³ In(n,α) ¹¹⁰ Ag ^m	249.8d	4.29	β-	98.64	446.812	3.62	N	N
¹¹³ In(n,α) ¹¹⁰ Ag ^m	249.8d	4.29	β-	98.64	620.3553	2.67	N	N
¹¹³ In(n,α) ¹¹⁰ Ag ^m	249.8d	4.29	β-	98.64	657.76	94.3	N	N
¹¹³ In(n,α) ¹¹⁰ Ag ^m	249.8d	4.29	β-	98.64	677.6217	10.56	N	N
¹¹³ In(n,α) ¹¹⁰ Ag ^m	249.8d	4.29	β-	98.64	687.0091	6.44	N	N
¹¹³ In(n,α) ¹¹⁰ Ag ^m	249.8d	4.29	β-	98.64	706.676	16.33	N	N
¹¹³ In(n,α) ¹¹⁰ Ag ^m	249.8d	4.29	β-	98.64	744.2755	4.77	N	N
¹¹³ In(n,α) ¹¹⁰ Ag ^m	249.8d	4.29	β-	98.64	763.9424	22.62	N	N
¹¹³ In(n,α) ¹¹⁰ Ag ^m	249.8d	4.29	β-	98.64	818.0244	7.34	N	N
¹¹³ In(n,α) ¹¹⁰ Ag ^m	249.8d	4.29	β-	98.64	884.6781	72.7	N	N
¹¹³ In(n,α) ¹¹⁰ Ag ^m	249.8d	4.29	β-	98.64	937.485	34.2	N	N
¹¹³ In(n,α) ¹¹⁰ Ag ^m	249.8d	4.29	β-	98.64	1384.2931	24.9	N	N
¹¹³ In(n,α) ¹¹⁰ Ag ^m	249.8d	4.29	β-	98.64	1475.7792	4.17	N	N
¹¹³ In(n,α) ¹¹⁰ Ag ^m	249.8d	4.29	β-	98.64	1505.028	13.6	N	N
¹¹³ In(n,α) ¹¹⁰ Ag ^m	249.8d	4.29	β-	98.64	1562.294	1.244	N	N
¹³⁹ La(n,γ) ¹⁴⁰ La	1.678d	99.91	β-	100	328.762	20.3	N	Y
¹³⁹ La(n,γ) ¹⁴⁰ La	1.678d	99.91	β-	100	432.493	2.9	N	Y
¹³⁹ La(n,γ) ¹⁴⁰ La	1.678d	99.91	β-	100	487.021	45.5	N	Y
¹³⁹ La(n,γ) ¹⁴⁰ La	1.678d	99.91	β-	100	751.637	4.33	N	Y
¹³⁹ La(n,γ) ¹⁴⁰ La	1.678d	99.91	β-	100	815.772	23.28	N	Y
¹³⁹ La(n,γ) ¹⁴⁰ La	1.678d	99.91	β-	100	867.846	5.5	N	Y
¹³⁹ La(n,γ) ¹⁴⁰ La	1.678d	99.91	β-	100	919.55	2.66	N	Y
¹³⁹ La(n,γ) ¹⁴⁰ La	1.678d	99.91	β-	100	925.189	6.9	N	Y
¹³⁹ La(n,γ) ¹⁴⁰ La	1.678d	99.91	β-	100	1596.21	95.4	N	Y
¹³⁹ La(n,γ) ¹⁴⁰ La	1.678d	99.91	β-	100	2521.4	3.46	N	Y
¹³⁹ La(n,2n) ¹³⁸ La	1.05 x 10 ¹¹ y	99.91	ε	65.6	1435.795	65.6	N	N
¹³⁹ La(n,2n) ¹³⁸ La	1.05 x 10 ¹¹ y	99.91	β-	34.4	788.742	34.4	N	N
¹³⁹ La(n,p) ¹³⁹ Ba	1.396h	99.91	β-	100	165.8575	24	N	N

Reaction	T _{1/2}	% natural	Decay	% Decay	γ energy [keV]	branching %	Visible with Pu-Be	ROI
¹³⁹ La(n,α) ¹³⁶ Cs	13.16d	99.91	β-	100	66.881	4.79	N	N
¹³⁹ La(n,α) ¹³⁶ Cs	13.16d	99.91	β-	100	86.36	5.18	N	N
¹³⁹ La(n,α) ¹³⁶ Cs	13.16d	99.91	β-	100	153.246	5.75	N	N
¹³⁹ La(n,α) ¹³⁶ Cs	13.16d	99.91	β-	100	163.92	3.39	N	N
¹³⁹ La(n,α) ¹³⁶ Cs	13.16d	99.91	β-	100	176.602	10	N	N
¹³⁹ La(n,α) ¹³⁶ Cs	13.16d	99.91	β-	100	273.646	11.1	N	N
¹³⁹ La(n,α) ¹³⁶ Cs	13.16d	99.91	β-	100	340.547	42.2	N	N
¹³⁹ La(n,α) ¹³⁶ Cs	13.16d	99.91	β-	100	818.514	99.704	N	N
¹³⁹ La(n,α) ¹³⁶ Cs	13.16d	99.91	β-	100	1048.073	80	N	N
¹³⁹ La(n,α) ¹³⁶ Cs	13.16d	99.91	β-	100	1235.362	20	N	N
¹³⁸ La(n,γ) ¹³⁹ La	stable	0.09						N
¹³⁸ La(n,2n) ¹³⁷ La	6 x 10 ⁴ y	0.09	no					N
¹³⁸ La(n,p) ¹³⁸ Ba	stable	0.09						N
¹³⁸ La(n,α) ¹³⁵ Cs ^m	53m	0.09	IT	100	787.2	100	N	N
¹³⁸ La(n,α) ¹³⁵ Cs ^m	53m	0.09	IT	100	846.1	96	N	N
⁵⁵ Mn(n,γ) ⁵⁶ Mn	2.578h	100	β-	100	846.754	98.9	Y	N
⁵⁵ Mn(n,γ) ⁵⁶ Mn	2.578h	100	β-	100	1810.72	27.2	Y	N
⁵⁵ Mn(n,γ) ⁵⁶ Mn	2.578h	100	β-	100	2113.05	14.3	Y	N
⁵⁵ Mn(n,2n) ⁵⁴ Mn	312.1d	100	ε	100	834.848	99.976	N	Y
⁵⁵ Mn(n,p) ⁵⁵ Cr	3.497m	100	all					N
⁵⁵ Mn(n,α) ⁵² V	3.76m	100	β-	100	1434.06	100	N	N
¹⁸¹ Ta(n,γ) ¹⁸² Ta	114.43d	99.988	β-	100	84.6808	2.65	N	Y
¹⁸¹ Ta(n,γ) ¹⁸² Ta	114.43d	99.988	β-	100	100.1065	14.1	N	Y
¹⁸¹ Ta(n,γ) ¹⁸² Ta	114.43d	99.988	β-	100	113.6725	1.88	N	Y
¹⁸¹ Ta(n,γ) ¹⁸² Ta	114.43d	99.988	β-	100	152.4308	6.93	N	Y
¹⁸¹ Ta(n,γ) ¹⁸² Ta	114.43d	99.988	β-	100	156.3876	2.64	N	Y
¹⁸¹ Ta(n,γ) ¹⁸² Ta	114.43d	99.988	β-	100	179.3945	3.08	N	Y
¹⁸¹ Ta(n,γ) ¹⁸² Ta	114.43d	99.988	β-	100	198.3532	1.44	N	Y
¹⁸¹ Ta(n,γ) ¹⁸² Ta	114.43d	99.988	β-	100	222.1096	7.49	N	Y
¹⁸¹ Ta(n,γ) ¹⁸² Ta	114.43d	99.988	β-	100	229.322	3.63	N	Y
¹⁸¹ Ta(n,γ) ¹⁸² Ta	114.43d	99.988	β-	100	264.0752	3.61	N	Y
¹⁸¹ Ta(n,γ) ¹⁸² Ta	114.43d	99.988	β-	100	1001.695	2.07	N	Y
¹⁸¹ Ta(n,γ) ¹⁸² Ta	114.43d	99.988	β-	100	1121.3008	34.9	N	Y
¹⁸¹ Ta(n,γ) ¹⁸² Ta	114.43d	99.988	β-	100	1189.0503	16.2	N	Y
¹⁸¹ Ta(n,γ) ¹⁸² Ta	114.43d	99.988	β-	100	1221.4066	27	N	Y
¹⁸¹ Ta(n,γ) ¹⁸² Ta	114.43d	99.988	β-	100	1231.0157	11.44	N	Y

Reaction	T _{1/2}	% natural	Decay	% Decay	γ energy [keV]	branching %	Visible with Pu-Be	ROI
¹⁸¹ Ta(n,γ) ¹⁸² Ta	114.43d	99.988	β-	100	1257.4185	1.49	N	Y
¹⁸¹ Ta(n,γ) ¹⁸² Ta	114.43d	99.988	β-	100	1289.1561	1.349	N	Y
¹⁸¹ Ta(n,γ) ¹⁸² Ta ^m	15.8m	99.988	IT	100	146.785	37.2	N	Y
¹⁸¹ Ta(n,γ) ¹⁸² Ta ^m	15.8m	99.988	IT	100	171.586	49	N	Y
¹⁸¹ Ta(n,γ) ¹⁸² Ta ^m	15.8m	99.988	IT	100	184.951	24.5	N	Y
¹⁸¹ Ta(n,γ) ¹⁸² Ta ^m	15.8m	99.988	IT	100	318.4	6.9	N	Y
¹⁸¹ Ta(n,2n) ¹⁸⁰ Ta	8.15h	99.988	ε	86	93.4	4.51	Y	N
¹⁸¹ Ta(n,p) ¹⁸¹ Hf	42.4d	99.988	β-	100	133.021	43.3	N	N
¹⁸¹ Ta(n,p) ¹⁸¹ Hf	42.4d	99.988	β-	100	136.26	5.85	N	N
¹⁸¹ Ta(n,p) ¹⁸¹ Hf	42.4d	99.988	β-	100	345.93	15.12	N	N
¹⁸¹ Ta(n,p) ¹⁸¹ Hf	42.4d	99.988	β-	100	482.18	80.5	N	N
¹⁸¹ Ta(n,α) ¹⁷⁸ Lu	28.5m	99.988	β-	100	93.179	6	N	N
¹⁸¹ Ta(n,α) ¹⁷⁸ Lu	28.5m	99.988	β-	100	1309.9	1.4	N	N
¹⁸¹ Ta(n,α) ¹⁷⁸ Lu	28.5m	99.988	β-	100	1340.8	3.42	N	N
¹⁸¹ Ta(n,α) ¹⁷⁸ Lu ^m	23.1m	99.988	β-	100	88.85	64.4	N	N
¹⁸¹ Ta(n,α) ¹⁷⁸ Lu ^m	23.1m	99.988	β-	100	93.15	17.2	N	N
¹⁸¹ Ta(n,α) ¹⁷⁸ Lu ^m	23.1m	99.988	β-	100	213.41	81.4	N	N
¹⁸¹ Ta(n,α) ¹⁷⁸ Lu ^m	23.1m	99.988	β-	100	216.64	2.48	N	N
¹⁸¹ Ta(n,α) ¹⁷⁸ Lu ^m	23.1m	99.988	β-	100	325.6	94.1	N	N
¹⁸¹ Ta(n,α) ¹⁷⁸ Lu ^m	23.1m	99.988	β-	100	331.62	11.4	N	N
¹⁸¹ Ta(n,α) ¹⁷⁸ Lu ^m	23.1m	99.988	β-	100	426.36	97	N	N
⁵¹ V(n,γ) ⁵² V	3.76m	99.75	β-	100	1434.06	100	N	N
⁵¹ V(n,2n) ⁵⁰ V	1.4 x 10 ¹⁷ y	99.75	β-	17	783.29	17	N	N
⁵¹ V(n,2n) ⁵⁰ V	1.4 x 10 ¹⁷ y	99.75	ε	83	1553.77	83	N	N
⁵¹ V(n,p) ⁵¹ Ti	5.76m	99.75	β-	100	320.076	93.1	N	N
⁵¹ V(n,p) ⁵¹ Ti	5.76m	99.75	β-	100	608.55	1.18	N	N
⁵¹ V(n,p) ⁵¹ Ti	5.76m	99.75	β-	100	928.63	6.9	N	N
⁵¹ V(n,α) ⁴⁸ Sc	43.7h	99.75	β-	100	175.361	7.48	N	Y
⁵¹ V(n,α) ⁴⁸ Sc	43.7h	99.75	β-	100	983.526	100.1	N	Y
⁵¹ V(n,α) ⁴⁸ Sc	43.7h	99.75	β-	100	1037.522	97.6	N	Y
⁵¹ V(n,α) ⁴⁸ Sc	43.7h	99.75	β-	100	1212.88	2.38	N	Y
⁵¹ V(n,α) ⁴⁸ Sc	43.7h	99.75	β-	100	1312.12	100.1	N	Y
⁵⁰ V(n,γ) ⁵¹ V	stable	0.25						N
⁵⁰ V(n,2n) ⁴⁹ V	331d	0.25	no					N
⁵⁰ V(n,p) ⁵⁰ Ti	stable	0.25						N
⁵⁰ V(n,α) ⁴⁷ Sc	3.349d	0.25	β-	100	159.381	68.3	N	N

Reaction	T _{1/2}	% natural	Decay	% Decay	γ energy [keV]	branching %	Visible with Pu-Be	ROI
⁵⁸ Ni(n,γ) ⁵⁹ Ni	7.6 x 10 ⁴ y	68.08	no					N
⁵⁸ Ni(n,2n) ⁵⁷ Ni	35.6h	68.08	β+	100	127.164	16.7	N	Y
⁵⁸ Ni(n,2n) ⁵⁷ Ni	35.6h	68.08	β+	100	1377.63	81.7	N	Y
⁵⁸ Ni(n,2n) ⁵⁷ Ni	35.6h	68.08	β+	100	1757.55	5.75	N	Y
⁵⁸ Ni(n,2n) ⁵⁷ Ni	35.6h	68.08	β+	100	1919.52	12.3	N	Y
⁵⁷ Ni - ⁵⁷ Co - ⁵⁷ Fe	271.8d	-	ε	100	122.06065	85.6	N	Y
⁵⁷ Ni - ⁵⁷ Co - ⁵⁷ Fe	271.8d	-	ε	100	136.47356	10.68	N	Y
⁵⁸ Ni(n,p) ⁵⁸ Co	70.88d	68.08	ε	100	810.7593	99.45	N	Y
⁵⁸ Ni(n,α) ⁵⁵ Fe	2.73y	68.08	no					N
⁶⁰ Ni(n,γ) ⁶¹ Ni	stable	26.22						N
⁶⁰ Ni(n,2n) ⁵⁹ Ni	7.6 x 10 ⁴ y	26.22	no					N
⁶⁰ Ni(n,p) ⁶⁰ Co	5.271y	26.22	β-	100	1173.228	99.85	N	N
⁶⁰ Ni(n,p) ⁶⁰ Co	5.271y	26.22	β-	100	1332.492	99.9826	N	N
⁶⁰ Ni(n,α) ⁵⁷ Fe	stable	26.22						N
⁶¹ Ni(n,γ) ⁶² Ni	stable	1.14						N
⁶¹ Ni(n,2n) ⁶⁰ Ni	stable	1.14						N
⁶¹ Ni(n,p) ⁶¹ Co	1.65h	1.14	β-	100	67.415	84.7	N	N
⁶¹ Ni(n,p) ⁶¹ Co	1.65h	1.14	β-	100	909.2	3.6	N	N
⁶¹ Ni(n,α) ⁵⁸ Fe	stable	1.14						N
⁶² Ni(n,γ) ⁶³ Ni	101y	3.63	no					N
⁶² Ni(n,2n) ⁶¹ Ni	stable	3.63						N
⁶² Ni(n,p) ⁶² Co	1.5m	3.63	β-	100	1128.9	11.1	N	N
⁶² Ni(n,p) ⁶² Co	1.5m	3.63	β-	100	1172.9	83.5	N	N
⁶² Ni(n,p) ⁶² Co	1.5m	3.63	β-	100	1985	1.6	N	N
⁶² Ni(n,p) ⁶² Co	1.5m	3.63	β-	100	2301.8	14.7	N	N
⁶² Ni(n,p) ⁶² Co	1.5m	3.63	β-	100	2345.9	1.3	N	N
⁶² Ni(n,p) ⁶² Co	13.9m	3.63	β-	99	777.5	1.72	N	N
⁶² Ni(n,p) ⁶² Co	13.9m	3.63	β-	99	875	1.28	N	N
⁶² Ni(n,p) ⁶² Co	13.9m	3.63	β-	99	1129	1.29	N	N
⁶² Ni(n,p) ⁶² Co	13.9m	3.63	β-	99	1163.5	68	N	N
⁶² Ni(n,p) ⁶² Co	13.9m	3.63	β-	99	1172.9	97.7	N	N
⁶² Ni(n,p) ⁶² Co	13.9m	3.63	β-	99	1718.7	6.7	N	N
⁶² Ni(n,p) ⁶² Co	13.9m	3.63	β-	99	2003.7	18.6	N	N
⁶² Ni(n,p) ⁶² Co	13.9m	3.63	β-	99	2104.7	6.4	N	N
⁶² Ni(n,p) ⁶² Co	13.9m	3.63	β-	99	2301.9	1.79	N	N
⁶² Ni(n,p) ⁶² Co	13.9m	3.63	β-	99	2882.3	1.09	N	N
⁶² Ni(n,α) ⁵⁹ Fe	44.5d	3.63	β-	100	142.651	1.02	N	N
⁶² Ni(n,α) ⁵⁹ Fe	44.5d	3.63	β-	100	192.343	3.08	N	N

Reaction	T _{1/2}	% natural	Decay	% Decay	γ energy [keV]	branching %	Visible with Pu-Be	ROI
⁶² Ni(n,α) ⁵⁹ Fe	44.5d	3.63	β-	100	1099.245	56.5	N	N
⁶² Ni(n,α) ⁵⁹ Fe	44.5d	3.63	β-	100	1291.59	43.2	N	N
⁶⁴ Ni(n,γ) ⁶⁵ Ni	2.517h	0.93	β-	100	366.27	4.81	N	N
⁶⁴ Ni(n,γ) ⁶⁵ Ni	2.517h	0.93	β-	100	1115.53	15.43	N	N
⁶⁴ Ni(n,γ) ⁶⁵ Ni	2.517h	0.93	β-	100	1481.84	23.59	N	N
⁶⁴ Ni(n,2n) ⁶³ Ni	101y	0.93	no					N
⁶⁴ Ni(n,p) ⁶⁴ Co	0.3s	0.93	β-	100	931.1	5	N	N
⁶⁴ Ni(n,p) ⁶⁴ Co	0.3s	0.93	β-	100	1346.1	10	N	N
⁶⁴ Ni(n,α) ⁶¹ Fe	6m	0.93	β-	100	120.34	5.3	N	N
⁶⁴ Ni(n,α) ⁶¹ Fe	6m	0.93	β-	100	177.61	2	N	N
⁶⁴ Ni(n,α) ⁶¹ Fe	6m	0.93	β-	100	297.9	22	N	N
⁶⁴ Ni(n,α) ⁶¹ Fe	6m	0.93	β-	100	1027.42	43	N	N
⁶⁴ Ni(n,α) ⁶¹ Fe	6m	0.93	β-	100	1205.07	44	N	N
⁶⁴ Ni(n,α) ⁶¹ Fe	6m	0.93	β-	100	1645.95	7	N	N
⁶⁴ Ni(n,α) ⁶¹ Fe	6m	0.93	β-	100	2011.6	4.4	N	N
⁶¹ Fe - ⁶¹ Co - ⁶¹ Ni	1.65h	1.14	β-	100	67.415	84.7	N	N
⁶¹ Fe - ⁶¹ Co - ⁶¹ Ni	1.65h	1.14	β-	100	909.2	3.6	N	N
⁶³ Cu(n,γ) ⁶⁴ Cu	12.701h	69.17	all					Y
⁶³ Cu(n,2n) ⁶² Cu	9.74m	69.17	all					N
⁶³ Cu(n,p) ⁶³ Ni	101y	69.17	no					N
⁶³ Cu(n,α) ⁶⁰ Co	5.271y	69.17	β-	100	1173.228	99.85	N	Y
⁶³ Cu(n,α) ⁶⁰ Co	5.271y	69.17	β-	100	1332.492	99.9826	N	Y
⁶⁵ Cu(n,γ) ⁶⁶ Cu	5.1m	30.83	β-	100	1039.2	9.23	N	N
⁶⁵ Cu(n,2n) ⁶⁴ Cu	12.701h	30.83	all					Y
⁶⁵ Cu(n,p) ⁶⁵ Ni	2.517h	30.83	β-	100	366.27	4.81	N	N
⁶⁵ Cu(n,p) ⁶⁵ Ni	2.517h	30.83	β-	100	1115.53	15.43	N	N
⁶⁵ Cu(n,p) ⁶⁵ Ni	2.517h	30.83	β-	100	1481.84	23.59	N	N
⁶⁵ Cu(n,α) ⁶² Co	1.5m	30.83	β-	100	1128.9	11.1	N	N
⁶⁵ Cu(n,α) ⁶² Co	1.5m	30.83	β-	100	1172.9	83.5	N	N
⁶⁵ Cu(n,α) ⁶² Co	1.5m	30.83	β-	100	1985	1.6	N	N
⁶⁵ Cu(n,α) ⁶² Co	1.5m	30.83	β-	100	2301.8	14.7	N	N
⁶⁵ Cu(n,α) ⁶² Co	1.5m	30.83	β-	100	2345.9	1.3	N	N
⁶⁵ Cu(n,α) ⁶² Co	13.9m	30.83	β-	99	777.5	1.72	N	N
⁶⁵ Cu(n,α) ⁶² Co	13.9m	30.83	β-	99	875	1.28	N	N
⁶⁵ Cu(n,α) ⁶² Co	13.9m	30.83	β-	99	1129	1.29	N	N
⁶⁵ Cu(n,α) ⁶² Co	13.9m	30.83	β-	99	1163.5	68	N	N
⁶⁵ Cu(n,α) ⁶² Co	13.9m	30.83	β-	99	1172.9	97.7	N	N

Reaction	T _{1/2}	% natural	Decay	% Decay	γ energy [keV]	branching %	Visible with Pu-Be	ROI
⁶⁵ Cu(n,α) ⁶² Co	13.9m	30.83	β-	99	1718.7	6.7	N	N
⁶⁵ Cu(n,α) ⁶² Co	13.9m	30.83	β-	99	2003.7	18.6	N	N
⁶⁵ Cu(n,α) ⁶² Co	13.9m	30.83	β-	99	2104.7	6.4	N	N
⁶⁵ Cu(n,α) ⁶² Co	13.9m	30.83	β-	99	2301.9	1.79	N	N
⁶⁵ Cu(n,α) ⁶² Co	13.9m	30.83	β-	99	2882.3	1.09	N	N

Appendix C. Point-to-Wire Solid Angle Comparison

The accurate counting of gamma rays has a major dependence on the geometry of the counting setup. The absolute efficiency of the counting system is the ratio of the number of gamma rays counted to the number of gamma rays emitted by the source. One factor of absolute efficiency is the solid angle subtended by the detector at the source position.

For a point source located along the axis of a right circular cylindrical detector, Figure 22, the solid angle (in steradians) is given by

$$\Omega = 2\pi\left(1 - \frac{d}{\sqrt{d^2 + a^2}}\right) \quad (19)$$

where d is the source-detector distance and a is the detector radius [12].

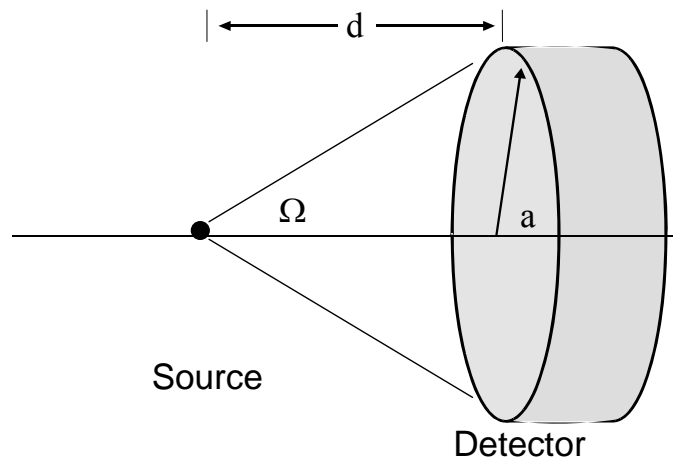


Figure 22. Solid angle for a point source.

The HPGe Canberra Model GC10021 detector has a crystal that is 83 mm in diameter so a is 41.5 mm. Plotting Equation 19 while varying d from 0 to 100 mm yields the curve in Figure 23. The plot passes the common sense test as it starts large and tapers off as the distance increases.

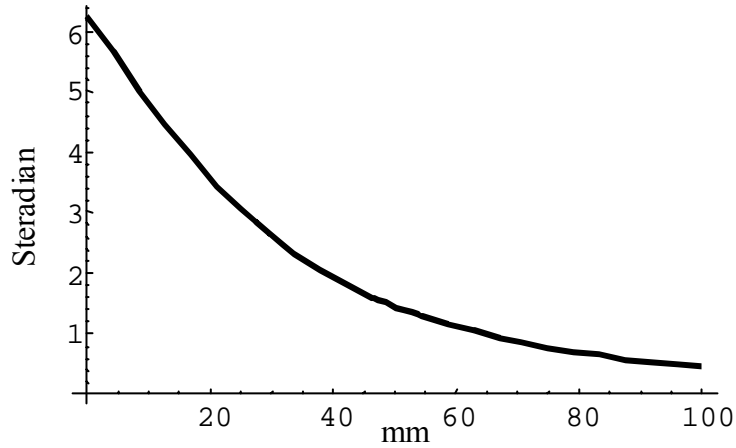


Figure 23. Point source solid angle vs. distance based on Knoll [12].

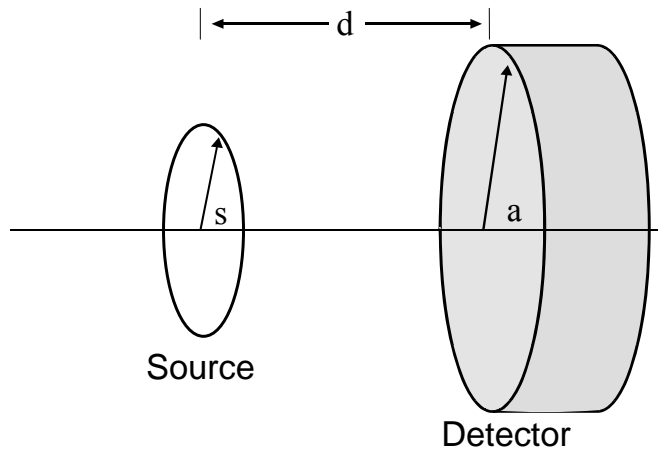


Figure 24. Solid angle geometry for a circular disk.

This thesis used wires instead of point sources. No equations could be found for wire geometry but several could be found for the more common disk geometry shown in Figure 24. A wire shows the detector a smaller surface than a disk with a diameter the same dimension as the length of the wire so the solid angle must also be smaller. Using the disk as a worst-case scenario and s as the radius of the source, it has been shown that

$$\Omega = \frac{2\pi a}{s} \int_0^\infty \frac{e^{-dk} J_1(sk) J_1(ak)}{k} dk \quad (20)$$

where the $J_1(x)$ are Bessel functions of x [12]. Since Equation 20 does not have an analytic solution, Knoll gives an approximation as shown in Figure 25 where the variables are as shown in Figure 24.

$$\alpha[\mathbf{d}] := \left(\frac{\mathbf{a}}{\mathbf{d}}\right)^2$$

$$\beta[\mathbf{d}] := \left(\frac{\mathbf{s}}{\mathbf{d}}\right)^2$$

$$\mathbf{F}_1[\mathbf{d}] := \frac{5}{16} \frac{\beta[\mathbf{d}]}{(1 + \beta[\mathbf{d}])^{7/2}} - \frac{35}{16} \frac{\beta[\mathbf{d}]^2}{(1 + \beta[\mathbf{d}])^{9/2}}$$

$$\mathbf{F}_2[\mathbf{d}] := \frac{35}{128} \frac{\beta[\mathbf{d}]}{(1 + \beta[\mathbf{d}])^{9/2}} - \frac{315}{256} \frac{\beta[\mathbf{d}]^2}{(1 + \beta[\mathbf{d}])^{11/2}} + \frac{1155}{1024} \frac{\beta[\mathbf{d}]^3}{(1 + \beta[\mathbf{d}])^{13/2}}$$

$$\Omega_c[\mathbf{d}] := 2\pi \left(1 - \frac{1}{(1 + \beta[\mathbf{d}])^{1/2}} - \frac{3}{8} \frac{\alpha[\mathbf{d}] \beta[\mathbf{d}]}{(1 + \beta[\mathbf{d}])^{5/2}} + \alpha[\mathbf{d}]^2 \mathbf{F}_1[\mathbf{d}] - \alpha[\mathbf{d}]^3 \mathbf{F}_2[\mathbf{d}] \right)$$

Figure 25. Approximation of solid angle for disk geometry based on Knoll [12].

Since the majority of wires used in this thesis are 1 cm long, the radius of the disk source is set at 5 mm. The radius of the detector remains at 41.5 mm. The plot of the approximation equation in Figure 25 for distances from 40 to 100 mm is given in Figure 26. It is obvious that this approximation is not accurate at shorter distances but appears to closely resemble the solid angle curve in Figure 23 from about 55 mm to at least 100 mm. For the detector used in this thesis, the crystal is 5 mm from the face of the detector and the wires are measured 1 mm above that for a total of 6 mm. The approximation does not work for this situation.

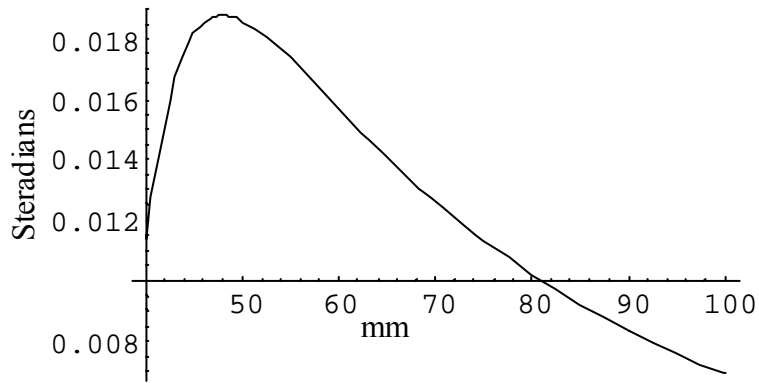


Figure 26. Approximation of disk solid angle vs. distance based on Knoll [12].

Ruby gives another approximation for disk geometry as shown in Figure 27 [21].

The variables are the same as in Knoll. Again, it is not accurate near the face of the detector but is a close approximation from about 40 mm to at least 100 mm as shown in

Figure 28. Again, this does not work with the distance of 6 mm.

$$\alpha[d] := \left(\frac{a}{d}\right)^2$$

$$\beta[d] := \left(\frac{s}{d}\right)^2$$

$$\Omega_x[d] :=$$

$$\pi * \alpha[d] \left(1 - \frac{3}{4} (\beta[d] - \alpha[d]) + \frac{15}{24} (\beta[d]^2 + \alpha[d]^2 + 3\beta[d] \alpha[d]) - \frac{35}{64} (\beta[d]^3 + \alpha[d]^3 + 6\beta[d] \alpha[d] (\beta[d] + \alpha[d])) \right)$$

Figure 27. Approximation of solid angle for disk geometry based on Ruby [21].

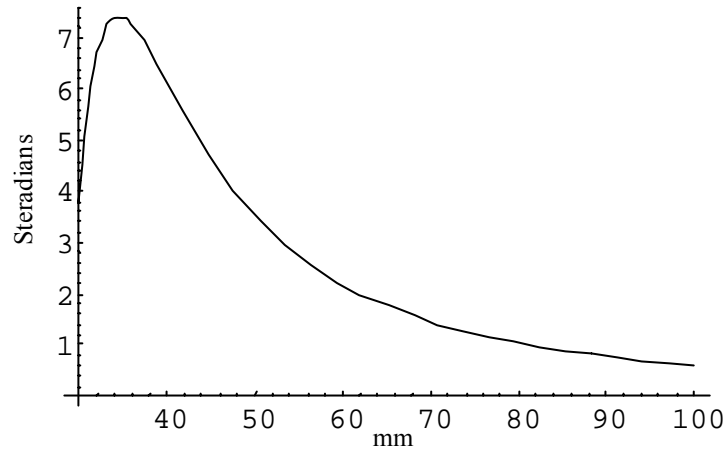


Figure 28. Approximation of disk solid angle vs. distance based on Ruby [21].

The integral of the Bessel functions in Equation 20 might not have analytic solutions but Mathematica[®] can easily approximate it using numerical techniques. Values were calculated using Mathematica[®] and Equations 19 and 20 from 1 mm to 1000 mm and the results tabulated in Table 12. Again, the detector radius was 41.5 mm and the source radius was 5 mm. The error maximized at about 35 mm. Closer than 35 mm the size of the detector overpowers the 1 cm disk and over 35 mm the disk appears increasingly like a point to the detector. At 1 mm off the surface of the detector where the wires are measured (6 mm overall), the difference in solid angle between a point and a 1 cm disk is less than 0.1%. Since a wire has a smaller solid angle than a disk, the difference would be even less. This amount of error is negligible when compared to the statistical error of spectroscopy.

Table 12. Point vs. disk solid angle comparison.

Comparison of Knoll (pg 118) point and disk solid angle equations

Calculations done in Mathematica

Detector radius = 41.5 mm

Source radius = 5 mm

<u>Distance (mm)</u>	Solid Angle		<u>% difference</u>
	<u>disk</u>	<u>point</u>	
1	6.1310092	6.1318271	0.01%
5	5.5276006	5.5316102	0.07%
6	5.3793851	5.3841208	0.09%
7	5.2327099	5.2381331	0.10%
8	5.0877981	5.093865	0.12%
9	4.944858	4.951522	0.13%
10	4.8040826	4.8112934	0.15%
15	4.1382386	4.1473868	0.22%
20	3.5455719	3.5553911	0.28%
25	3.0314569	3.0409823	0.31%
30	2.5935465	2.6022	0.33%
35	2.2248674	2.2323981	0.34%
40	1.9164368	1.9228116	0.33%
50	1.4440195	1.4483921	0.30%
60	1.1127091	1.1156496	0.26%
70	0.8764548	0.8784413	0.23%
80	0.7044239	0.7057867	0.19%
90	0.5764273	0.5773808	0.17%
100	0.4792129	0.4798939	0.14%
102	0.4626302	0.4632684	0.14%
125	0.3197317	0.3200513	0.10%
150	0.2273252	0.2274918	0.07%
200	0.1309911	0.1310482	0.04%
250	0.0847964	0.0848207	0.03%
500	0.0215296	0.0215312	0.01%
1000	0.0054035	0.0054036	0.00%

Appendix D. Wire Activation Simulation Results

Table 13. Calculations to determine wire size.

	($\sigma\phi$) SCALE [n/s]	density [g/cm ³]	radius [cm]	length [cm]	volume [cm ³]	mass [mg]	# of atoms target	# of atoms activated	activity [Bq]	T½ [days]	λ [1/d]	A at +4 days [Bq]
Al												
500 m	6.26 x 10 ⁻¹³	2.70	0.05	1.00	7.85 x 10 ⁻³	21.20	4.73 x 10 ²⁰	2.96 x 10 ⁸	3815.97	0.62	1.11	4.46 x 10 ¹
330 m	3.24 x 10 ⁻¹²	2.70	0.05	0.05	3.71 x 10 ⁻⁴	1.00	2.23 x 10 ¹⁹	7.24 x 10 ⁷	932.27	0.62	1.11	1.09 x 10 ¹
700 m	2.07 x 10 ⁻¹³	2.70	0.05	1.00	7.85 x 10 ⁻³	21.20	4.73 x 10 ²⁰	9.78 x 10 ⁷	1259.02	0.62	1.11	1.47 x 10 ¹
800 m	7.64 x 10 ⁻¹⁴	2.70	0.05	1.00	7.85 x 10 ⁻³	21.20	4.73 x 10 ²⁰	3.61 x 10 ⁷	465.41	0.62	1.11	5.44
1000 m	1.84 x 10 ⁻¹⁴	2.70	0.05	1.00	7.85 x 10 ⁻³	21.20	4.73 x 10 ²⁰	8.69 x 10 ⁶	111.95	0.62	1.11	1.31
2500 m	5.78 x 10 ⁻¹⁹	2.70	0.05	1.00	7.85 x 10 ⁻³	21.20	4.73 x 10 ²⁰	2.73 x 10 ²	0.00	0.62	1.11	4.11 x 10 ⁻⁵
Au												
500 m	9.46 x 10 ⁻¹²	19.30	0.05	0.30	2.36 x 10 ⁻³	45.47	1.39 x 10 ²⁰	1.32 x 10 ⁹	1707.56	6.18	1.12 x 10 ⁻¹	1.09 x 10 ³
1000 m	2.52 x 10 ⁻¹³	19.30	0.05	0.30	2.36 x 10 ⁻³	45.47	1.39 x 10 ²⁰	3.50 x 10 ⁷	45.47	6.18	1.12 x 10 ⁻¹	2.90 x 10 ¹
1100 m	1.85 x 10 ⁻¹³	19.30	0.05	0.30	2.36 x 10 ⁻³	45.47	1.39 x 10 ²⁰	2.57 x 10 ⁷	33.33	6.18	1.12 x 10 ⁻¹	2.13 x 10 ¹
1200 m	6.22 x 10 ⁻¹⁴	19.30	0.05	0.30	2.36 x 10 ⁻³	45.47	1.39 x 10 ²⁰	8.65 x 10 ⁶	11.22	6.18	1.12 x 10 ⁻¹	7.17
2500 m	4.91 x 10 ⁻¹⁸	19.30	0.05	0.30	2.36 x 10 ⁻³	45.47	1.39 x 10 ²⁰	6.82 x 10 ²	0.00	6.18	1.12 x 10 ⁻¹	5.65 x 10 ⁻⁴
Co												
500 m	6.24 x 10 ⁻¹¹	8.90	0.05	1.00	7.85 x 10 ⁻³	69.90	7.14 x 10 ²⁰	4.46 x 10 ¹⁰	185.90	1923.92	3.60 x 10 ⁻⁴	1.86 x 10 ²
1000 m	1.05 x 10 ⁻¹¹	8.90	0.05	1.00	7.85 x 10 ⁻³	69.90	7.14 x 10 ²⁰	7.50 x 10 ⁹	31.25	1923.92	3.60 x 10 ⁻⁴	3.12 x 10 ¹
1100 m	3.80 x 10 ⁻¹²	8.90	0.05	1.00	7.85 x 10 ⁻³	69.90	7.14 x 10 ²⁰	2.72 x 10 ⁹	11.33	1923.92	3.60 x 10 ⁻⁴	1.13 x 10 ¹
1200 m	8.38 x 10 ⁻¹³	8.90	0.05	1.00	7.85 x 10 ⁻³	69.90	7.14 x 10 ²⁰	5.99 x 10 ⁸	2.50	1923.92	3.60 x 10 ⁻⁴	2.49
2500 m	1.30 x 10 ⁻¹⁵	8.90	0.05	1.00	7.85 x 10 ⁻³	69.90	7.14 x 10 ²⁰	9.27 x 10 ⁵	0.00	1923.92	3.60 x 10 ⁻⁴	3.86 x 10 ⁻³
In												
100 m	1.22 x 10 ⁻⁹	7.31	0.05	1.00	7.85 x 10 ⁻³	57.41	3.01 x 10 ²⁰	3.69 x 10 ¹¹	1.58 x 10 ⁷	0.19	3.71	5.73
200 m	2.89 x 10 ⁻¹⁰	7.31	0.05	1.00	7.85 x 10 ⁻³	57.41	3.01 x 10 ²⁰	8.70 x 10 ¹⁰	3.73 x 10 ⁶	0.19	3.71	1.35
300 m	1.09 x 10 ⁻¹⁰	7.31	0.05	1.00	7.85 x 10 ⁻³	57.41	3.01 x 10 ²⁰	3.28 x 10 ¹⁰	1.41 x 10 ⁶	0.19	3.71	5.10 x 10 ⁻¹
500 m	2.49 x 10 ⁻¹¹	7.31	0.05	1.00	7.85 x 10 ⁻³	57.41	3.01 x 10 ²⁰	7.50 x 10 ⁹	3.22 x 10 ⁵	0.19	3.71	1.17 x 10 ⁻¹
1000 m	1.75 x 10 ⁻¹²	7.31	0.05	1.00	7.85 x 10 ⁻³	57.41	3.01 x 10 ²⁰	5.27 x 10 ⁸	2.26 x 10 ⁴	0.19	3.71	8.20 x 10 ⁻³
2500 m	7.62 x 10 ⁻¹⁷	7.31	0.05	1.00	7.85 x 10 ⁻³	57.41	3.01 x 10 ²⁰	2.29 x 10 ⁴	0.98	0.19	3.71	3.57 x 10 ⁷
La												
500 m	1.15 x 10 ⁻¹¹	6.15	0.05	0.50	3.93 x 10 ⁻³	24.13	1.05 x 10 ²⁰	1.20 x 10 ⁹	5747.28	1.68	4.13 x 10 ⁻¹	1.10 x 10 ³
1000 m	5.31 x 10 ⁻¹²	6.15	0.05	0.50	3.93 x 10 ⁻³	24.13	1.05 x 10 ²⁰	5.55 x 10 ⁸	2654.46	1.68	4.13 x 10 ⁻¹	5.09 x 10 ²
1600 m	2.72 x 10 ⁻¹³	6.15	0.05	0.50	3.93 x 10 ⁻³	24.13	1.05 x 10 ²⁰	2.85 x 10 ⁷	136.26	1.68	4.13 x 10 ⁻¹	2.61 x 10 ¹
1700 m	1.32 x 10 ⁻¹⁴	6.15	0.05	0.50	3.93 x 10 ⁻³	24.13	1.05 x 10 ²⁰	1.39 x 10 ⁶	6.62	1.68	4.13 x 10 ⁻¹	1.27
2500 m	1.29 x 10 ⁻¹⁴	6.15	0.05	0.50	3.93 x 10 ⁻³	24.13	1.05 x 10 ²⁰	1.35 x 10 ⁶	6.48	1.68	4.13 x 10 ⁻¹	1.24
Mn 80%												
500 m	2.71 x 10 ⁻¹²	7.30	0.05	1.50	1.18 x 10 ⁻²	68.80	7.54 x 10 ²⁰	2.05 x 10 ⁹	52.60	312.10	2.22 x 10 ⁻³	5.21 x 10 ¹
700 m	5.23 x 10 ⁻¹³	7.30	0.05	1.50	1.18 x 10 ⁻²	68.80	7.54 x 10 ²⁰	3.95 x 10 ⁸	10.14	312.10	2.22 x 10 ⁻³	1.01 x 10 ¹
1000 m	4.56 x 10 ⁻¹⁴	7.30	0.05	1.50	1.18 x 10 ⁻²	68.80	7.54 x 10 ²⁰	3.44 x 10 ⁷	0.88	312.10	2.22 x 10 ⁻³	8.75 x 10 ¹
1200 m	7.90 x 10 ⁻¹⁵	7.30	0.05	1.50	1.18 x 10 ⁻²	68.80	7.54 x 10 ²⁰	5.96 x 10 ⁶	0.15	312.10	2.22 x 10 ⁻³	1.52 x 10 ¹
2500 m	3.61 x 10 ⁻¹⁸	7.30	0.05	1.50	1.18 x 10 ⁻²	68.80	7.54 x 10 ²⁰	2.73 x 10 ³	0.00	312.10	2.22 x 10 ⁻³	6.94 x 10 ⁻⁵
Ta												
500 m	3.83 x 10 ⁻¹⁰	16.65	0.02	0.50	5.67 x 10 ⁻⁴	9.44	3.14 x 10 ¹⁹	1.21 x 10 ¹⁰	844.82	114.43	6.06 x 10 ⁻³	8.25 x 10 ²
1000 m	6.65 x 10 ⁻¹¹	16.65	0.02	0.50	5.67 x 10 ⁻⁴	9.44	3.14 x 10 ¹⁹	2.09 x 10 ⁹	146.42	114.43	6.06 x 10 ⁻³	1.43 x 10 ²
1100 m	1.33 x 10 ⁻¹¹	16.65	0.02	0.50	5.67 x 10 ⁻⁴	9.44	3.14 x 10 ¹⁹	4.18 x 10 ⁸	29.33	114.43	6.06 x 10 ⁻³	2.86 x 10 ¹
1200 m	7.73 x 10 ⁻¹²	16.65	0.02	0.50	5.67 x 10 ⁻⁴	9.44	3.14 x 10 ¹⁹	2.43 x 10 ⁸	17.04	114.43	6.06 x 10 ⁻³	1.66 x 10 ¹
1300 m	5.36 x 10 ⁻¹²	16.65	0.02	0.50	5.67 x 10 ⁻⁴	9.44	3.14 x 10 ¹⁹	1.68 x 10 ⁸	11.80	114.43	6.06 x 10 ⁻³	1.15 x 10 ¹
2500 m	6.82 x 10 ⁻¹⁹	16.65	0.02	0.50	5.67 x 10 ⁻⁴	9.44	3.14 x 10 ¹⁹	2.14 x 10 ¹	0.00	114.43	6.06 x 10 ⁻³	1.47 x 10 ⁻⁶
V												
500 m	6.23 x 10 ⁻¹⁴	6.11	0.05	1.00	7.85 x 10 ⁻³	47.99	5.67 x 10 ²⁰	3.53 x 10 ⁷	155.61	1.82	3.81 x 10 ⁻¹	3.40 x 10 ¹
600 m	3.38 x 10 ⁻¹⁴	6.11	0.05	1.00	7.85 x 10 ⁻³	47.99	5.67 x 10 ²⁰	1.92 x 10 ⁷	84.41	1.82	3.81 x 10 ⁻¹	1.84 x 10 ¹
700 m	1.60 x 10 ⁻¹⁴	6.11	0.05	1.00	7.85 x 10 ⁻³	47.99	5.67 x 10 ²⁰	9.08 x 10 ⁶	40.00	1.82	3.81 x 10 ⁻¹	8.73
1000 m	1.75 x 10 ⁻¹⁵	6.11	0.05	1.00	7.85 x 10 ⁻³	47.99	5.67 x 10 ²⁰	9.95 x 10 ⁵	4.38	1.82	3.81 x 10 ⁻¹	9.57 x 10 ¹
2500 m	1.58 x 10 ⁻²⁰	6.11	0.05	1.00	7.85 x 10 ⁻³	47.99	5.67 x 10 ²⁰	8.96	0.00	1.82	3.81 x 10 ⁻¹	8.61 x 10 ⁻⁶

	($\sigma\phi$) SCALE [n/s]	density [g/cm ³]	radius [cm]	length [cm]	volume [cm ³]	mass [mg]	# of atoms target	# of atoms activated	activity [Bq]	T½ [days]	λ [1/d]	A at +4 days [Bq]
Ni	cross-section for (n,p)											
500 m	3.67×10^{-12}	8.90	0.05	1.00	7.85×10^{-3}	69.92	7.17×10^{20}	2.63×10^9	298.12	70.88	9.78×10^{-3}	2.87×10^2
1000 m	1.57×10^{-13}	8.90	0.05	1.00	7.85×10^{-3}	69.92	7.17×10^{20}	1.13×10^8	12.74	70.88	9.78×10^{-3}	1.22×10^1
1100 m	9.82×10^{-14}	8.90	0.05	1.00	7.85×10^{-3}	69.92	7.17×10^{20}	7.05×10^7	7.97	70.88	9.78×10^{-3}	7.67
2500 m	7.22×10^{-18}	8.90	0.05	1.00	7.85×10^{-3}	69.92	7.17×10^{20}	5.18×10^3	0.00	70.88	9.78×10^{-3}	5.63×10^{-4}
Cu	cross-section for (n,a)											
250 m	1.61×10^{-12}	8.96	0.05	2.00	1.57×10^{-2}	140.74	1.33×10^{21}	2.14×10^9	8.93	1923.92	3.60×10^{-4}	8.92
300 m	9.69×10^{-13}	8.96	0.05	2.00	1.57×10^{-2}	140.74	1.33×10^{21}	1.29×10^9	5.39	1923.92	3.60×10^{-4}	5.38
500 m	1.51×10^{-13}	8.96	0.05	2.00	1.57×10^{-2}	140.74	1.33×10^{21}	2.02×10^8	0.84	1923.92	3.60×10^{-4}	8.40×10^1
1000 m	2.70×10^{-15}	8.96	0.05	2.00	1.57×10^{-2}	140.74	1.33×10^{21}	3.60×10^6	0.02	1923.92	3.60×10^{-4}	1.50×10^2
2500 m	8.70×10^{-20}	8.96	0.05	2.00	1.57×10^{-2}	140.74	1.33×10^{21}	1.16×10^2	0.00	1923.92	3.60×10^{-4}	4.83×10^{-7}

Table 14. MCNP calculations to verify SCALE at 500 meters.

Energy Group [MeV]	MCNP [1/cm ²]	Initial Neutrons	Total Flux [n/cm ²]	Cross-section SCALE [b]	Convert to [cm ²]	Flux times cross-section	Target Atoms 1mg	atoms activated
14	1.758×10^{-12}	1.000×10^{24}	1.758×10^{12}	1.226×10^{-1}	1.223×10^{-25}	2.155×10^{-13}	2.233×10^{19}	4.812×10^6
13.84	1.938×10^{-12}	1.000×10^{24}	1.938×10^{12}	1.279×10^{-1}	1.279×10^{-25}	2.478×10^{-13}	2.233×10^{19}	5.533×10^6
12.84	2.023×10^{-12}	1.000×10^{24}	2.023×10^{12}	1.116×10^{-1}	1.116×10^{-25}	2.257×10^{-13}	2.233×10^{19}	5.040×10^6
10	6.342×10^{-13}	1.000×10^{24}	6.342×10^{11}	6.643×10^{-2}	6.643×10^{-26}	4.213×10^{-14}	2.233×10^{19}	9.407×10^5
8.1873	9.948×10^{-13}	1.000×10^{24}	9.948×10^{11}	1.976×10^{-2}	1.976×10^{-26}	1.966×10^{-14}	2.233×10^{19}	4.389×10^5
6.434	1.734×10^{-12}	1.000×10^{24}	1.734×10^{12}	7.053×10^{-4}	7.053×10^{-28}	1.223×10^{-15}	2.233×10^{19}	2.732×10^4
4.8	6.904×10^{-13}	1.000×10^{24}	6.904×10^{11}	1.521×10^{-7}	1.521×10^{-31}	1.050×10^{-19}	2.233×10^{19}	2.345
4.304	1.535×10^{-12}	1.000×10^{24}	1.535×10^{12}	2.908×10^{-11}	2.908×10^{-35}	4.464×10^{-23}	2.233×10^{19}	9.967×10^{-4}
3	1.814×10^{-11}	1.000×10^{24}	1.814×10^{13}	0.000	0.000	0.000	2.233×10^{19}	
			2.944×10^{13}				Total Activation	1.679×10^7

Appendix E. Calculation of N₂O Steel Cylinder Activation

One concern when irradiating through equipment and supporting materials is the resulting activation. The N₂O cylinder was to be placed in direct line with the beam port so would receive a full dose of neutrons. The activity induced could cause handling the cylinder to be hazardous and require special storage and disposition of the cylinder.

Of particular interest was the activation of ⁵⁸Fe to ⁵⁹Fe with a half-life of 44.5 days, which in turn decays to ⁵⁹Co. Iron-58 can be gained from the activation of ⁵⁷Fe that can be gained from the activation of ⁵⁶Fe and so forth all the way back to ⁵⁴Fe.

Calculations show that the gain in ⁵⁸Fe from the chain of lower irons is negligible in comparison to the amount of ⁵⁸Fe initially on hand, even though ⁵⁸Fe is only 0.282% of natural iron. An example of this calculation done in Mathematica[®] is shown at the end of this appendix.

The N₂O container was composed of 4130 steel (97.56% iron) with sidewalls of 0.5 cm [9, 32]. The cylinder was 20.01 cm in diameter and 51 cm high. The cylinder was placed upright against the end of the beam port. The beam was collimated to make it appear as a point source. Only part of the steel cylinder was in direct line of the neutron beam as shown in Figure 29.

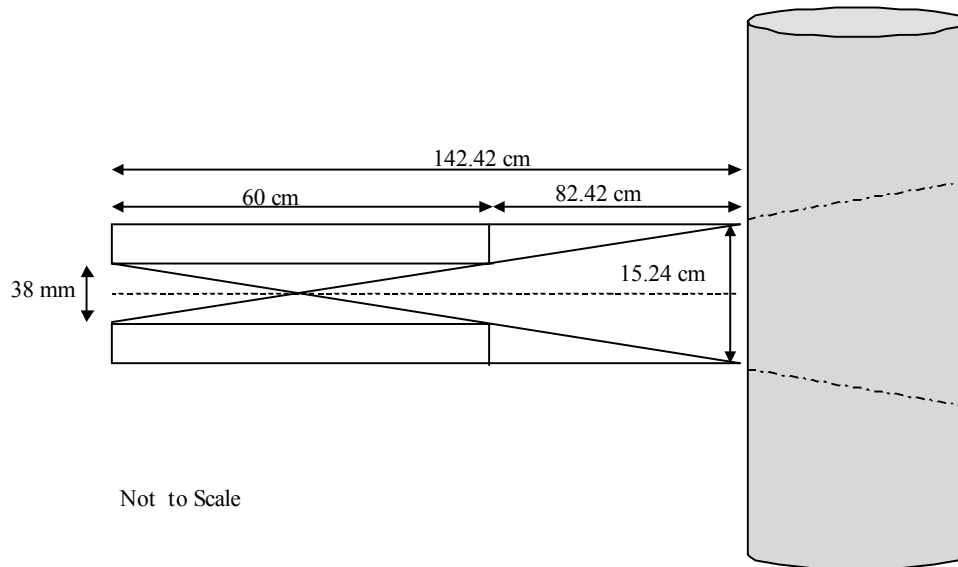


Figure 29. Geometry of cylinder at OSU beam port.

The volume of the cylinder in the direct path of neutrons can be estimated by multiplying the thickness by the surface area involved shown by the beam projections in Figure 29. The height of the area of interest at the back of the cylinder is calculated from using like triangles as in Figure 30. Since the height solved for is half the projected height, the complete height is 17.95 cm.

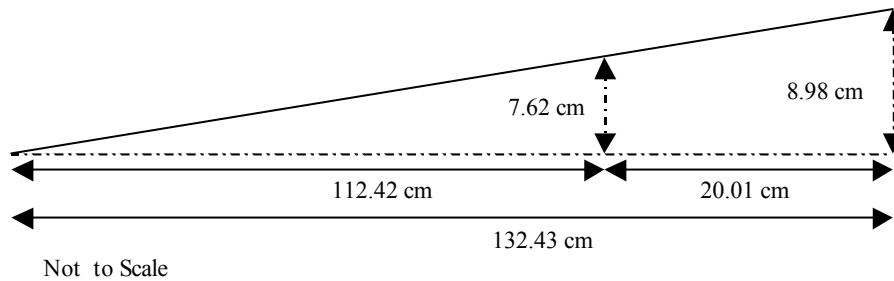


Figure 30. Using like triangles to solve projected height.

Vertically splitting the area of interest at the shortest part and unrolling the cylinder, gives an estimated flattened area as shown in Figure 31. This area is then easily calculated to give 1043.6 cm^2 and an associated volume of 521.8 cm^3 .

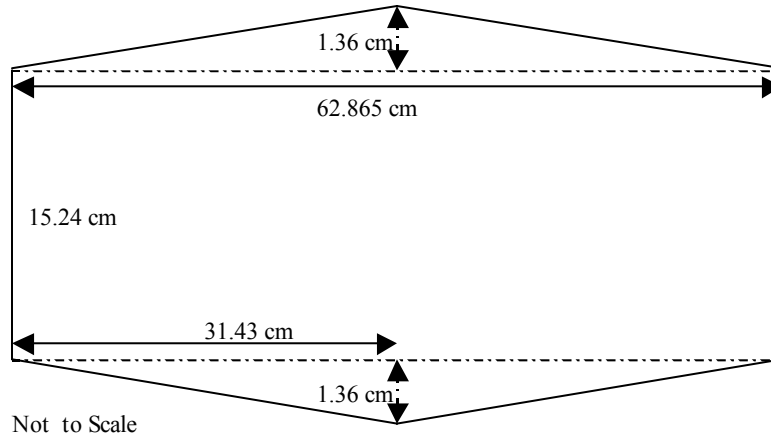


Figure 31. Estimated area of activation.

This area is only an approximation of what will be activated. Some scattering will occur so areas outside the direct path will receive some activation. The flux will be attenuated somewhat between the front of the cylinder and the back so the activation will not be evenly distributed. The approximation is only used for getting an idea of the activation of cylinder for safety planning.

Activity is

$$A = \lambda N = \Phi \sigma N_T (1 - e^{-\lambda t}) \quad (21)$$

where:

A = activity

$$\lambda = \text{decay constant} = \frac{\ln 2}{\text{half-life}}$$

Φ = fluence rate [$\text{cm}^{-2} \text{s}^{-1}$]

σ = cross section [b] or [10^{-24}cm^2]

N_T = target nuclei

t = time of irradiation [28].

The thermal cross-section (σ_γ) is applied for neutron energies of approximately 0.5 eV and lower. For higher energy values, the resonance integral (RI) is used to represent the probability of neutron reactions. Common practice uses the RI just like a

cross-section [3]. For ^{58}Fe , $\sigma_\gamma = 1.3 \text{ b}$ and $\text{RI} = 1.2 \text{ b}$. The half-life of ^{59}Fe is 44.5 days

or 1068 hours leading to $\lambda = \frac{\ln 2}{1068h} = 6.49 \times 10^{-4}/h$.

Radiation will be for 7 hours at 450 kW (90% power). The number of target nuclei is calculated from

$$N_T = \frac{\rho N_A}{AW} V(\%) \quad (22)$$

where:

$\rho = \text{density} = 7.874 \text{ g cm}^{-3}$

$N_A = \text{Avogadro's constant} = 6.0221 \times 10^{23} \text{ nuclei mol}^{-1}$

$AW = \text{atomic weight} = 59 \text{ g mol}^{-1}$

$V = \text{volume} = 521.8 \text{ cm}^3$

$\% = \% \text{ of composition} = (0.00282)(.9756)$.

This gives an N_T of 1.15×10^{23} ^{58}Fe nuclei. At the end of the 205 cm beam port closest to the core the flux is $7.8 \times 10^{12} \text{ n cm}^{-2} \text{ s}^{-1}$ of which $4.5 \times 10^{12} \text{ n cm}^{-2} \text{ s}^{-1}$ is considered thermal [11]. Of the total flux, 57.7% is thermal and 42.3% is fast. This is at 100% power. For safety reasons, the maximum operating level used is 90% so the flux will be:

$$\Phi_{\text{th}} = 4.05 \times 10^{12} \text{ n cm}^{-2} \text{ s}^{-1}$$

$$\Phi_{\text{fast}} = 2.97 \times 10^{12} \text{ n cm}^{-2} \text{ s}^{-1}.$$

The flux must be calculated at the open end of the beam port so, assuming no scattering and a uni-directional flux, the flux can be divided by distance² to get an estimation. The distance is 205 cm so:

$$\Phi_{\text{th}} = 9.64 \times 10^7 \text{ n cm}^{-2} \text{ s}^{-1}$$

$$\Phi_{\text{fast}} = 7.07 \times 10^7 \text{ n cm}^{-2} \text{ s}^{-1}.$$

Then using Equation 21 and the appropriate cross section or resonance integral gives:

$$A_{th} = (9.64 \times 10^7 \text{ n cm}^{-2} \text{ s}^{-1})(1.3 \times 10^{-24} \text{ cm}^2)(1.15 \times 10^{23})(1 - e^{-(0.000649/h)(7 \text{ h})})$$

$$A_{th} = 6.53 \times 10^4/\text{s}$$

$$A_{fast} = (7.07 \times 10^7 \text{ n cm}^{-2} \text{ s}^{-1})(1.2 \times 10^{-24} \text{ cm}^2)(1.15 \times 10^{23})(1 - e^{-(0.000649/h)(7 \text{ h})})$$

$$A_{fast} = 4.42 \times 10^4/\text{s} .$$

This gives a total activity of $1.10 \times 10^5/\text{s}$ or 2.96 mCi.

Sample Mathematica[®] calculations for iron activation to ⁵⁹Fe.

Fe-54 → 1

Fe-55 → 2

Fe-56 → 3

Fe-57 → 4

Fe-58 → 5

Fe-59 → 6

n_i → initial number of atoms

n_{\square} → number of atoms

σ_{\square} → cross section

ϕ → flux

Assumptions: Flux is from SCALE at 2×10^7 . Decay from Fe-55 is negligible since it has a half-life of 2.73 years and it is only coming from Fe-54. 7 hour radiation time = 25200 seconds. No initial Fe-59.

$$\text{DSolve}[n_2' [t] == \sigma_1 * \phi * n_{i1} - \sigma_2 * \phi * n_2' [t], n_2[t], t]$$

$$\left\{ \left\{ n_2[t] \rightarrow C[1] + \frac{t \phi n_{i1} \sigma_1}{1 + \phi \sigma_2} \right\} \right\}$$

$$\text{DSolve}[n_3' [t] == \sigma_2 * \phi * n_2[t] - \sigma_3 * \phi * (n_{i3} + n_3' [t]), n_3[t], t]$$

$$\left\{ \left\{ n_3[t] \rightarrow C[1] + \int_{K\$761}^t \frac{-\phi n_{i3} \sigma_3 + \phi \sigma_2 n_2[K\$760]}{1 + \phi \sigma_3} dK\$760 \right\} \right\}$$

$$\text{DSolve}[n_4' [t] == \sigma_3 * \phi * n_3[t] - \sigma_4 * \phi * (n_{i4} + n_4' [t]), n_4[t], t]$$

$$\left\{ \left\{ n_4[t] \rightarrow C[1] + \int_{K\$1418}^t \frac{-\phi n_{i4} \sigma_4 + \phi \sigma_3 n_3[K\$1417]}{1 + \phi \sigma_4} dK\$1417 \right\} \right\}$$

$$\text{DSolve}[n_5' [t] == \sigma_4 * \phi * n_4[t] - \sigma_5 * \phi * (n_{i5} + n_5' [t]), n_5[t], t]$$

$$\left\{ \left\{ n_5[t] \rightarrow C[1] + \int_{K\$2097}^t \frac{-\phi n_{i5} \sigma_5 + \phi \sigma_4 n_4[K\$2096]}{1 + \phi \sigma_5} dK\$2096 \right\} \right\}$$

$$\text{DSolve}[n_6' [t] == \sigma_5 * \phi * n_5[t] - \lambda * n_6[t], n_6[t], t]$$

$$\left\{ \left\{ n_6[t] \rightarrow e^{-t\lambda} C[1] + e^{-t\lambda} \int_{K\$2771}^t e^{K\$2770\lambda} \phi \sigma_5 n_5[K\$2770] dK\$2770 \right\} \right\}$$

$$\sigma_1 = 2.3 * 10^{-24};$$

$$\phi = 2 * 10^7;$$

$$n_{i1} = 2.142 * 10^{24};$$

$$\sigma_2 = 13 * 10^{-24};$$

$$\sigma_3 = 2.6 * 10^{-24};$$

$$\sigma_4 = 2.5 * 10^{-24};$$

$$\sigma_5 = 1.3 * 10^{-24};$$

$$n_{i3} = 3.243 * 10^{25};$$

$$n_{i4} = 7.358 * 10^{23};$$

$$n_{i5} = 9.624 * 10^{22};$$

$$\lambda = 1.803 * 10^{-7};$$

$$\text{DSolve}[n_2'[t] == \sigma_1 * \phi * n_{i1} - \sigma_2 * \phi * n_2'[t], n_2[t], t]$$

$$\left\{ \left\{ n_2[t] \rightarrow 9.853199999999999 \times 10^7 t + C[1] \right\} \right\}$$

$$9.853199999999999 \cdot 10^7 * 25200$$

$$2.4830064 \times 10^{12}$$

$$\text{DSolve}[n_3'[t] == \sigma_2 * \phi * 2.4830063999999995 \cdot 10^{12} - \sigma_3 * \phi * (n_{i3} + n_3'[t]),$$

$$n_3[t], t]$$

$$\left\{ \left\{ n_3[t] \rightarrow -1.6863599999999355 \times 10^9 t + C[1] \right\} \right\}$$

$$-1.68635999999993546 \cdot 10^9 * 25200 + 3.243 * 10^{25}$$

$$3.242999999995751 \times 10^{25}$$

$$\text{DSolve}[n_4'[t] == \sigma_3 * \phi * 3.2429999999957505 \cdot 10^{25} - \sigma_4 * \phi * (n_{i4} + n_4'[t]),$$

$$n_4[t], t]$$

$$\left\{ \left\{ n_4[t] \rightarrow 1.64956999999779 \times 10^9 t + C[1] \right\} \right\}$$

$$1.6495699999977903 \cdot 10^9 * 25200 + 7.358 * 10^{23}$$

$$7.35800000041569 \times 10^{23}$$

$$\text{DSolve}[n_5'[t] == \sigma_4 * \phi * 7.35800000041569 \cdot 10^{23} - \sigma_5 * \phi * (n_{i5} + n_5'[t]),$$

$$n_5[t], t]$$

$$\left\{ \left\{ n_5[t] \rightarrow 3.428776000207846 \times 10^7 t + C[1] \right\} \right\}$$

$$3.428776000207846 \cdot 10^7 * 25200 + 9.624 * 10^{22}$$

$$9.624000000086405 \times 10^{22}$$

$$\text{DSolve}[n_6'[t] == \sigma_5 * \phi * 9.624000000086405 \cdot 10^{22} - \lambda * n_6[t],$$

$$n_6[t], t]$$

$$\left\{ \left\{ n_6[t] \rightarrow 1.387820299513292 \times 10^{13} \right. \right.$$

$$\left. \left. 2.718281828459045 \cdot 1.803 \times 10^{-7} t e^{-1.803 \times 10^{-7} t} + e^{-1.803 \times 10^{-7} t} C[1] \right\} \right\}$$

$$1.3878202995132922 \times 10^{13} \cdot e^{-1.8029999999999997 \times 10^{-7} \cdot 25200}$$

$$1.387820299513292 \times 10^{13}$$

Activity (Bq):

$$1.3878202995132922 \times 10^{13} \cdot \lambda$$

$$2.502240000022466 \times 10^6$$

Activity (Ci):

$$2.502240000022466 \times 10^6 / (3.7 \times 10^{10})$$

$$0.0000676281081087153$$

Bibliography

1. Anderson, M.E. "Increases in Neutron Yields of Plutonium-Beryllium (α,n) Sources." *Nuclear Applications*, 4: 142-147 (1968).
2. Anderson, M.E. and R.A. Neff. "Neutron Energy Spectra of $^{239}\text{Pu-Be}$ (α,n) Sources." *Nuclear Instruments and Methods*, 99: 231-235 (1972).
3. Baum, Edward, Harold Knox and Thomas Miller. *Nuclides and Isotopes*, 16th ed. Lockheed Martin, 2002.
4. Broadhead, Bryan. Sr. Development Staff, Reactor and Fuel Cycle Analysis, Computational Physics and Engineering Division. Oak Ridge National Laboratory, Oak Ridge TN. Personal correspondence, June 2004.
5. Canberra Industries Inc. "747 Series Lead Shield." Product webpage. http://www.canberra.com/pdf/Products/Detectors_pdf/747.pdf. 29 December 2004.
6. -----. *Genie 2000 Spectroscopy System*. Meriden CT: Canberra Industries, 2001.
7. -----. "Germanium Detectors Brochure," *Canberra online*. <http://www.canberra.com/literature/945.asp>. 25 July 2004.
8. Glasstone, Samuel and Philip Dolan. *The Effects of Nuclear Weapons*, 3rd ed. Washington: United States Department of Defense and United States Department of Energy, 1977.
9. Hydrospin. "Sec. 178.37 Specification 3AA and 3AAX seamless steel cylinders." Product information, manufacturing specs. http://www.hydrospin.com/product_info/178_3AA.doc. 23 November 2004.
10. Jones, Kent. Chief of Academics and Instruction, Defense Nuclear Weapons School, DTRA, Kirtland Air Force Base NM. Personal correspondence, July 2004.
11. Kauffman, Andrew. Ohio State University Research Reactor, Columbus OH. Personal correspondence. December 2004.
12. Knoll, Glenn. *Radiation Detection and Measurement*, 3rd ed. New York: John Wiley & Sons, 2000.

13. Krane, Kenneth. *Introductory Nuclear Physics*. New York: John Wiley & Sons, 1988.
14. Lillie, Richard. Oak Ridge National Laboratory, Oak Ridge TN. Personal correspondence. July 2004.
15. Mollendorff, U.V. and others. *A Nuclear Simulation Experiment for the International Fusion Materials Irradiation Facility (IFMIF)*. Karlsruhe, Germany: Forschungszentrum Karlsruhe GmbH, 2002.
16. Monsanto Research Corporation. "Plutonium Neutron Source Shipping Documents for Neutron Source M-1170". Mound Laboratory: Miamisburg OH, 9 March 1962.
17. National Nuclear Data Center. "Decay Radiation Search." NuDat 2.1. http://www.nndc.bnl.gov/nudat2/indx_dec.jsp. 27 November 2004.
18. NIST. "X-ray Mass Coefficients," *NIST online*. <http://physics.nist.gov/PhysRefData/XrayMassCoef/cover.html>. 10 July 2004.
19. ORTEC. "The Best Choice of High Purity Germanium (HPGe) Detector," *ORTEC Online*. http://www.ortec-online.com/pdf/best_choice/det.pdf. 25 July 2004.
20. Petrosky, James C. Air Force Institute of Technology, Dayton OH. Personal correspondence. January 2005.
21. Ruby, Lawrence. "Further Comments on the Geometrical Efficiency of a Parallel-Disk Source and Detector System." *Nuclear Instruments and Methods in Physics Research A*, 337: 531-533 (1994).
22. Santoro, R. and others. *Progress Report – Active Interrogation Integrated Detector System (AFIDS)*. Oak Ridge National Laboratory, Oak Ridge TN, 2003.
23. "SCALE homepage." <http://www.ornl.gov/sci/scale/>. 6 January 2005.
24. Silicon Carbide Products. "SCProbond™ N." <http://www.scprobond.com>. 20 November 2004.
25. Stanford, George S. and James H. Seckinger. *Thickness Corrections for Neutron-Activated Gold Foils*. Springfield VA: Clearing House for Federal Scientific and Technical Information, National Bureau of Standards, U.S. Department of Commerce, February 1969.

26. Talnagi, Joseph. Ohio State University Research Reactor, Columbus OH. Personal correspondence. November 2004.
27. Tang, J. S. and M. B. Emmett. *SAS4: A Monte Carlo Cask Shielding Analysis Module Using an Automated Biasing Procedure*. NUREG/CR-0200, Vol. 1, Section S4, Revision 6. Washington: U.S. Nuclear Regulatory Commission, March 2000.
28. Turner, James. *Atoms, Radiation, and Radiation Protection*, 2nd ed. New York: John Wiley & Sons, 1995.
29. Uhlman, Troy. MS student, Air Force Institute of Technology, Dayton OH. Personal correspondence, December 2004.
30. Vaughn, Stephanie. *Investigation of a Passive, Temporal, Neutron Monitoring System That Functions Within the Confines of START I*. MS Thesis, AFIT/GNE/ENP/03-10. Graduate School of Engineering and Management, Air Force Institute of Technology (AU), Wright-Patterson AFB OH, March 2003.
31. Weast, Robert. *Handbook of Chemistry and Physics*, 57th ed. Cleveland: Chemical Rubber Publishing Company, 1976.
32. Wedding, Jim. Customer service representative, Taylor-Wharton Corporation. Personal correspondence. November 2004.
33. Whitworth, Paul F. Jr. *Determination of Pu-Be Source Strength by Manganese Activation*. MS Thesis, AFIT/GNE/ENP/88M-10. Graduate School of Engineering and Management, Air Force Institute of Technology (AU), Wright-Patterson AFB OH, March 1988.

Vita

Captain Warren E. Kimmel graduated from Montana State University in Bozeman, Montana with a Bachelor of Science degree in Electrical and Electronic Engineering Technology. Following his commissioning into the United States Army as an Ordnance Officer, he was assigned to the 302nd Forward Support Battalion, 2nd Infantry Division at Camp Casey, Korea. He served as a platoon leader and direct support maintenance shop officer.

Captain Kimmel's next assignment was with the 541st Maintenance Battalion, 937th Engineer Group at Fort Riley, Kansas. He served as the executive officer of 1st Maintenance Company and as the 541st Battalion S3 operations officer.

Following the Combined Logistics Captains Career Course, Captain Kimmel was assigned to the 501st Corps Support Group in Camp Red Cloud, Korea. After six months as the personnel officer, he took command of the Headquarters and Headquarters Detachment, 498th Maintenance Battalion in Yongsan, Korea. Captain Kimmel was selected to attend the School of Engineering and Management, Air Force Institute of Technology. Captain Kimmel's next assignment will be to the Defense Threat Reduction Agency.

REPORT DOCUMENTATION PAGE			Form Approved OMB No. 074-0188		
The public reporting burden for this collection of information is estimated to average 1 hour per response, including the time for reviewing instructions, searching existing data sources, gathering and maintaining the data needed, and completing and reviewing the collection of information. Send comments regarding this burden estimate or any other aspect of the collection of information, including suggestions for reducing this burden to Department of Defense, Washington Headquarters Services, Directorate for Information Operations and Reports (0704-0188), 1215 Jefferson Davis Highway, Suite 1204, Arlington, VA 22202-4302. Respondents should be aware that notwithstanding any other provision of law, no person shall be subject to a penalty for failing to comply with a collection of information if it does not display a currently valid OMB control number. PLEASE DO NOT RETURN YOUR FORM TO THE ABOVE ADDRESS.					
1. REPORT DATE (DD-MM-YYYY) March 2005		2. REPORT TYPE Master's Thesis		3. DATES COVERED (From - To) March 2004 - March 2005	
4. TITLE AND SUBTITLE MANUFACTURE AND TESTING OF AN ACTIVATION FOIL PACKAGE FOR USE IN AFIDS			5a. CONTRACT NUMBER		
			5b. GRANT NUMBER		
			5c. PROGRAM ELEMENT NUMBER		
6. AUTHOR(S) Kimmel, Warren E., Captain, USA			5d. PROJECT NUMBER ENR #137-01		
			5e. TASK NUMBER		
			5f. WORK UNIT NUMBER		
7. PERFORMING ORGANIZATION NAMES(S) AND ADDRESS(S) Air Force Institute of Technology Graduate School of Engineering and Management (AFIT/EN) 2950 Hobson Way, Building 640 WPAFB OH 45433-8865			8. PERFORMING ORGANIZATION REPORT NUMBER AFIT/GNE/ENP/05-06		
9. SPONSORING/MONITORING AGENCY NAME(S) AND ADDRESS(ES) DTRA HEADQUARTERS ATTN: 1 st LT Lakesha Stevenson DTRA/CSNN 8725 John J. Kingman Road Ft. Belvoir, VA 22060-6201			10. SPONSOR/MONITOR'S ACRONYM(S)		
			11. SPONSOR/MONITOR'S REPORT NUMBER(S)		
12. DISTRIBUTION/AVAILABILITY STATEMENT APPROVED FOR PUBLIC RELEASE; DISTRIBUTION UNLIMITED.					
13. SUPPLEMENTARY NOTES					
14. ABSTRACT <p>This study used simulation and experiment to design and test foil packets for use in the Activation Foil Integrated Detection System (AFIDS). The initial plan to activate foil packets outside with the pulse reactor at White Sands Missile Range (WSMR) was not possible due to WSMR not having safety approval to take the reactor outside. As an alternative, the concept of using liquid nitrous oxide inside a reactor to simulate large volumes of air was investigated.</p> <p>Simulation using the Standardized Computer Analyses for Licensing Evaluation (SCALE) program was used to select ten foils to be included in the foil packet. The size was selected with a target activity of 25 Bq for each foil four days after the activation when located 500 meters from a five kiloton equivalent neutron weapon.</p> <p>We analyzed whether N₂O could replicate large volumes of air in neutron transport experiments since one cubic centimeter of liquid N₂O contains as many molecules as 1371 cubic centimeters of air. A neutron propagating through the liquid N₂O should react like a neutron propagating through 1371 times as much air. Actual testing could not be completed at the Ohio State University Research Reactor due to hazardous levels of radiation in the facility during testing. The results of the simulation showed that pragmatic experimental factors inhibit use of the reactor in this way and an outside test is still required to provide the information Oak Ridge National Laboratory (ORNL) needs to validate the methodology used in Domestic Nuclear Event Attribution (DNEA).</p>					
15. SUBJECT TERMS Neutron Activation, Foils(Materials), Spectroscopy, Computerized Simulation					
16. SECURITY CLASSIFICATION OF:			17. LIMITATION OF ABSTRACT UU	18. NUMBER OF PAGES 94	19a. NAME OF RESPONSIBLE PERSON James C. Petrosky, Dr.
a. REPORT U	b. ABSTRACT U	c. THIS PAGE U			19b. TELEPHONE NUMBER (Include area code) (937) 255-3636, ext 4562 (james.petrosky@afit.edu)